Published as: *Geochim Cosmochim Acta*. 2010 May 10; 74(10): 2826–2842.

Evidence for equilibrium iron isotope fractionation by nitrate-reducing iron(II)-oxidizing bacteria

A. Kappler[1,2,*], **C.M. Johnson**[3,4], **H.A. Crosby**[3], **B.L. Beard**[3,4], and **D.K. Newman**[1,5]

[1] GPS Division, California Institute of Technology, Pasadena, CA 91125

[3] Department of Geology and Geophysics, University of Wisconsin-Madison, 1215 West Dayton Street, Madison, Wisconsin 53706

[4] NASA Astrobiology Institute

Abstract

Iron isotope fractionations produced during chemical and biological Fe(II) oxidation are sensitive to the proportions and nature of dissolved and solid-phase Fe species present, as well as the extent of isotopic exchange between precipitates and aqueous Fe. Iron isotopes therefore potentially constrain the mechanisms and pathways of Fe redox transformations in modern and ancient environments. In the present study, we followed in batch experiments Fe isotope fractionations between $Fe(II)_{aq}$ and Fe(III) oxide/hydroxide precipitates produced by the Fe(III) mineral encrusting, nitrate-reducing, Fe (II)-oxidizing *Acidovorax* sp. strain BoFeN1. Isotopic fractionation in $^{56}Fe/^{54}Fe$ approached that expected for equilibrium conditions, assuming an equilibrium $\Delta^{56}Fe_{Fe(OH)3 - Fe(II)aq}$ fractionation factor of +3.0 ‰. Previous studies have shown that Fe(II) oxidation by this *Acidovorax* strain occurs in the periplasm, and we propose that Fe isotope equilibrium is maintained through redox cycling via coupled electron and atom exchange between $Fe(II)_{aq}$ and Fe(III) precipitates in the contained environment of the periplasm. In addition to the apparent equilibrium isotopic fractionation, these experiments also record the kinetic effects of initial rapid oxidation, and possible phase transformations of the Fe(III) precipitates. Attainment of Fe isotope equilibrium between Fe(III) oxide/hydroxide precipitates and $Fe(II)_{aq}$ by neutrophilic, Fe(II)-oxidizing bacteria or through abiologic $Fe(II)_{aq}$ oxidation is generally not expected or observed, because the poor solubility of their metabolic product, i.e. Fe(III), usually leads to rapid precipitation of Fe(III) minerals, and hence expression of a kinetic fractionation upon precipitation; in the absence of redox cycling between Fe $(II)_{aq}$ and precipitate, kinetic isotope fractionations are likely to be retained. These results highlight the distinct Fe isotope fractionations that are produced by different pathways of biological and abiological Fe(II) oxidation.

1 Introduction

Iron redox cycling is a significant process in many aquatic and terrestrial environments and plays a key role in determining the fate of nutrients (e.g., P, N), metal ions (e.g., arsenate and

*To whom correspondence should be sent: Andreas Kappler, andreas.kappler@uni-tuebingen.de, Geomicrobiology, Center for Applied Geosciences, University of Tübingen, D-72076 Tübingen, Germany.
[2]Now: Geomicrobiology, Center for Applied Geosciences, University of Tübingen, D-72076 Tübingen, Germany
[5]Now: Departments of Biology and Earth, Atmospheric and Planetary Sciences, Massachusetts Institute of Technology, Cambridge, MA 02139

chromate), and organic compounds (Ehrlich, 2008; Zachara et al., 2001; Neubauer et al., 2008). At neutral pH, Fe(III) is poorly soluble and mostly present in the form of iron (hydr) oxides such as ferrihydrite ($Fe(OH)_3$), goethite (FeOOH), hematite (Fe_2O_3), and magnetite (Fe_3O_4) (Cornell and Schwertmann, 2003). Fe(II) is stable under anoxic conditions and present either as dissolved species or in the form of iron(II) minerals such as Fe-carbonate (e.g., siderite, $FeCO_3$) or Fe-phosphate (e.g., vivianite, $Fe_3(PO_4)_2$). Abiotic pathways of Fe redox cycling include chemical reduction of Fe(III) (e.g., by sulfide) and chemical oxidation of Fe(II) (e.g., by O_2). Iron redox cycling may also be driven by biologically catalyzed processes (Kappler and Straub, 2005; Weber et al., 2006). Microorganisms are known to be able to respire Fe(III) minerals by transferring electrons stemming from oxidation of hydrogen or organic electron donors to Fe(III) (Lovley, 2004). Additionally, neutrophilic, aerobic Fe(II)-oxidizing microorganisms can compete with chemical oxidation of Fe(II) by O_2 (Emerson and Moyer, 1997). Even under neutrophilic anoxic conditions, bacteria can grow via oxidation of Fe(II) either by using light as an energy source for CO_2-fixation (phototrophic Fe(II) oxidation; Widdel et al., 1993; Ehrenreich and Widdel, 1994), or by using nitrate as an electron acceptor (nitrate-dependent Fe(II) oxidation; Straub et al., 1996; Hafenbradl et al., 1996).

Both aerobic and anaerobic iron-oxidizing microorganisms that oxidize Fe(II) at circumneutral pH face the problem of the extremely poor solubility of Fe(III), one of the end products of their metabolism. At circumneutral pH, the ambient concentration of dissolved Fe(III) in solution is typically in the nM to μM range (Stumm and Morgan 1995), and at this pH, the Fe(III) minerals formed during precipitation are positively charged due to their high points of net zero charge (pzc ~7.9 for ferrihydrite and pzc ~9.0–9.4 for goethite; Schwertmann and Cornell, 2000; pzc ~8.5 for hematite; Jeon et al., 2004). If formed by microbial Fe(II) oxidation, Fe(III) ions, Fe(III) colloids and Fe(III) minerals would therefore be expected to adsorb to the cell surface, which is in general negatively charged due to a high content of carboxylic, phosphoryl and/or hydroxyl groups. This could lead to cell encrustation, potentially limiting the diffusion of substrates and nutrients to the cell, impairing uptake of these compounds across the membrane, and, as a consequence, leading to stagnation of cell metabolism and eventually to cell death.

For stalk- or sheath-forming aerobic Fe(II)-oxidizing bacteria of the genera *Gallionella* and *Leptothrix*, it was suggested that microbially produced and excreted organic matrices are used for extra-cellular precipitation/binding of Fe(III) minerals produced during aerobic Fe(II) oxidation (Hanert 1981; Emerson and Revsbech 1994). This, however, still leaves open the questions i) where is Fe(II) oxidized (in the cytoplasm, in the periplasm, or at the cell surface?), and ii) in the case of intracellular oxidation, how is Fe(III) transported from the cytoplasm to the cell surface and the organic templates? Abiologic Fe(II) oxidation is often envisioned to occur at circum-neutral pH via a “two-step-model”, where Fe(II) oxidation generates an intermediate Fe(III) species that then precipitates in a second step as an Fe(III) mineral, but it remains unknown if neutrophilic Fe(II)-oxidizing bacteria follow the same path. Recent studies indicate that different strains of neutrophilic Fe(II)-oxidizing microorganisms utilize different mechanisms and exhibit different biomineralization patterns, particularly with respect to the importance of dissolved Fe(III) (Kappler and Newman, 2004; Kappler et al., 2005; Hegler et al., 2008; Miot et al., 2009, Schaedler et al., 2009). For example, the nitrate-reducing, iron-oxidizing β-proteobacterial strain BoFeN1 becomes encrusted with Fe(III) minerals as iron oxidation proceeds (Kappler et al., 2005; Schaedler et al., 2009; Miot et al., 2009; Fig. 1), whereas the photosynthetic iron-oxidizing purple bacteria *Rhodobacter ferroxidans* strain SW2 (Ehrenreich and Widdel, 1994) and *Thiodictyon* sp. strain F4 (Croal et al., 2004; Fig. 1) do not encrust, even after complete oxidation of Fe(II) (Kappler and Newman, 2004; Schaedler et al., 2009). It has been suggested that this is related to differences in Fe(II) oxidation and Fe(III) stabilization (solubilization) mechanisms, yet the exact mechanisms accounting for these two distinct phenotypes are still poorly understood.

Bacterial species may use several strategies to avoid encrustation of the cell surface with the Fe(III) minerals they produce, although these are only speculative (Schaedler et al., 2009). It was suggested that phototrophic Fe(II)-oxidizing bacteria oxidize Fe(II) at the cell surface (Ehrenreich and Widdel, 1994), allowing Fe(III) minerals to fall away from the cell surface, but this does not explain how the electrons are then transported from the outside to the inside of the cell and why the positively charged Fe(III) minerals do not bind to the negatively charged cell surface. Recently it was proposed that Fe(II) oxidation by the photoautotrophic strains "*Rhodobacter ferrooxidans"* strain SW2 and *Rhodopseudomonas palustris* strain TIE-1, occurs in the periplasm of the cells (Croal et al. 2007; Jiao et al. 2007). Because cell encrustation was not observed in these strains (Kappler and Newman 2004; Jiao et al. 2005; Schaedler et al., 2009), it remains unclear how Fe(III) is transported after periplasmic Fe(II) oxidation to the cell exterior and then away from the cells. The possibility of a low-pH microenvironment was suggested for strain SW2 (Kappler and Newman 2004), as well as for neutrophilic aerobic Fe(II)-oxidizers (Sobolev and Roden 2001). A lower pH would potentially keep Fe(III) in solution in close cell proximity and lead to controlled Fe(III) mineral precipitation at a certain distance from the cell surface. A role for organic ligands as complexing and solubilization agents has also been postulated (Croal et al. 2004), although no evidence for such molecules has been found so far.

Isotopic studies have great potential for providing insight into bacterial redox cycling, as has been demonstrated, for example, using S and Fe isotopes (e.g. Farquhar and Wing, 2003; Johnson et al., 2004a; Johnson et al., 2004b). In most low-temperature aqueous environments, the largest Fe isotope fractionations occur between Fe(III) and Fe(II) species (e.g. Schauble et al., 2001; Welch et al., 2003). In addition, chloride speciation may change Fe isotope fractionations on the order of 0.2 ‰/M Cl^- in $^{56}Fe/^{54}Fe$ ratios (e.g., Hill and Schauble, 2008), and isotopic fractionations up to 1 ‰ are predicted or measured between aqueous Fe and Fe complexed by organic ligands (e.g., Domagal-Goldman and Kubicki, 2008; Dideriksen et al., 2008). Iron isotope fractionation during bacterial Fe(II) oxidation has been investigated in experiments on anaerobic photosynthetic Fe(II)-oxidizing bacteria at circum-neutral pH, where CO_2 was the terminal electron acceptor (Croal et al., 2004). The Fe isotope fractionations produced by bacterial Fe(II) oxidation in acidic and oxic conditions have been studied by Balci et al. (2006), where O_2 was the terminal electron acceptor and significant quantities of dissolved Fe(III) were produced. In the experiments of Croal et al. (2004) and Balci et al. (2006), the ferric hydroxide precipitates did not encrust the cells, and in the case of the work by Balci et al. (2006), Fe(II) oxidation clearly occurred via a two-step process of oxidation of Fe(II) to Fe (III), followed by precipitation of Fe(III) as $Fe(OH)_3$. Croal et al. (2004) inferred oxidation and precipitation via a two-step process, but the presence of dissolved Fe(III) was not detected in the ambient solution. Because isotopic exchange between $Fe(III)_{aq}$ and $Fe(II)_{aq}$ is very rapid (Johnson et al., 2002; Welch et al., 2003), where complete isotopic exchange may occur in less than one minute, isotopic equilibrium is expected to be maintained between aqueous Fe species even under conditions of extremely rapid oxidation, although kinetic fractionations produced upon precipitation may still occur (Beard and Johnson, 2004), indicating the overall isotopic fractionation between ferric oxide/hydroxide precipitates and $Fe(II)_{aq}$ may be dependent upon precipitation rates.

The goal of the current study was to determine the Fe isotope fractionations produced via biological oxidation of Fe(II) by a recently isolated nitrate-dependent Fe(II)-oxidizing strain (*Acidovorax* sp. strain BoFeN1; Kappler at al, 2005). Relative to the previous studies of Croal et al. (2004) and Balci et al. (2006), where the cells did not become encrusted with ferric hydroxide mineral products, oxidation of Fe(II) by *Acidovorax* forms crusts of iron(III) (hydr) oxides in the periplasm and at the cell surface as Fe(II) oxidation proceeds, suggesting a potentially different pathway for Fe(III) mineral formation compared to previous studies (Miot et al. (2009)). The results reported here indicate that different Fe isotope fractionations may

be produced by a variety of microbial Fe(II) oxidation processes, and these may depend on the extent of Fe redox cycling in intra-cellular micro environments.

2 Methods

2.1. Media and growth conditions

Acidovorax sp. strain BoFeN1 was cultivated as described previously (Kappler et al., 2005). The anoxic medium was buffered at pH 6.8 with bicarbonate (30 mM). Vitamin and trace-element solutions (1 ml each) and a vitamin B_{12} solution (1 ml) were added anoxically under a gas stream of N_2:CO_2 (v:v, 80:20) (for details and concentrations see Ehrenreich and Widdel, 1994). The medium was transferred into an anoxic glove box, and 5–10 ml of an anoxic 1 M $FeCl_2$ stock solution were added followed by precipitation of a whitish-grey precipitate, which, based on earlier work (Croal et al., 2004), probably consisted of vivianite and siderite that formed from phosphate and bicarbonate present in the medium. After 24 h the medium was filtered (0.2 μm, cellulose nitrate, Millipore), leaving a clear solution that contained ~2–6 mM of aqueous Fe(II). In uninoculated controls, no further precipitation was observed for the duration of the incubations. This method allowed isotope analysis of the Fe(III) precipitates formed by the Fe(II)-oxidizing bacteria in the absence of Fe(II) precipitates in the background, which is critical for determining the actual $Fe(II)_{aq}$-ferric oxide/hydroxide fractionation factors. The medium (25 ml) was transferred anoxically into 58-ml serum bottles that were closed with butyl rubber stoppers, crimped and flushed with N_2-CO_2 (v:v, 80:20). Acetate (2 mM final concentration) as organic co-substrate and nitrate (5 mM final concentration) as electron acceptor were added from anoxic stock solutions (see also Kappler et al., 2005). Cultures were incubated at 16 and 30°C for 21 days.

Iron speciation analysis for the filtered medium was calculated using Geochemists Workbench 6.05 (minteq database). The calculation yielded $[Fe(H_2O)_6]^{2+}$ (81.6%), $[FeHCO_3]^+$ (10.1%), $FeSO_{4aq}$ (5.6%), [Fe-acetate]$^+$ (1.6%), $[FeCl]^+$ (0.4%), $[FeHPO_4]_{aq}$ (0.4%), $[FeH_2PO4]^+$ (0.2%), and $[FeOH]^+$ (0.1%) as the main aqueous Fe species present. These calculations indicate that the Fe isotope effects due to variable aqueous speciation were negligible, and the measured $Fe(II)_{aq}$ - ferric oxide/hydroxide fractionations may be assumed to be equal to $[Fe(H_2O)_6]^{2+}$ - ferric oxide/hydroxide fractionations. Although the second most abundant species is $[FeHCO_3]^+$, we infer only small fractionations between $[FeHCO_3]^+$ and $[Fe(H_2O)_6]^{2+}$ based on the small (+0.5 ‰) fractionation in $^{56}Fe/^{54}Fe$ between $[Fe(H_2O)_6]^{2+}$ and siderite ($FeCO_3$) at room temperature (Wiesli et al., 2004), suggesting an effect of <0.05 ‰ given the proportion of $[FeHCO_3]^+$. The effects of Cl^- and acetate speciation on the measured Fe isotope fractionations have been calculated by Hill and Schauble (2008) and Ottonello and Vetuschi Zuccolini (2008) and these are insignificant at the levels that existed in the experiments.

2.2. Wet chemical and spectrophotometrical Fe(II) and Fe(III) analysis

For analysis of dissolved iron ($Fe(II)_{aq}$), a 200 μl culture suspension was withdrawn in an anoxic glovebox with a syringe and filtered through Nylon (0.22 μm) filter tubes (Costar, Corning, NY). The filtrate was acidified with 1 M HCl to stabilize the solutions and analyzed spectrophotometrically outside the glove box for total dissolved Fe and dissolved Fe(II) using *Ferrozine* assay after incubation in the presence or absence of the reducing agent hydroxylamine hydrochloride (Stookey, 1970). For analysis of total iron, a 100 μl suspension was added in the glove box to 900 μl 6 M HCl, and incubated for 1 h. After filtration through 0.22 μm Nylon filter tubes (Costar, Corning, NY) in the glove box, total Fe and Fe(II) concentrations were determined as above. All iron measurements by the *Ferrozine* assay were done in triplicate. The standard deviation (SD) for these triplicate measurements was usually smaller than the SD calculated for different independent experiments. Dissolved Fe(III) may be estimated as the difference between total dissolved Fe and dissolved Fe(II); in all cases total

Fe and Fe(II) contents were identical within uncertainty of the calibration curves, indicating that dissolved Fe(III) contents were insignificant. Sorbed Fe(II) contents were determined from the solids collected after centrifugation of 1-ml aliquots of culture suspension. The pellets were washed twice in anoxic water (in the anoxic glove box), followed by extraction using a solution of 0.5 M sodium acetate (NaAc) and acidification by 1 M HCl prior to spectrophotometric analysis outside the anoxic chamber, which stabilized the solutions. Total and Fe(II) contents were determined on the water washes, and these contained several μM Fe(II) and Fe(III), which likely reflects small amounts of sorbed Fe(II) and Fe(III) precipitates, but these quantities were insignificant. Measurement of total Fe and Fe(II) contents of the NaAc extractions indicated that all Fe in these extracts was Fe(II). The percent oxidation for each sample was calculated based on the sum of $Fe(II)_{aq}$ and $Fe(II)_{sorb}$, relative to the initial $FeCl_2$ contents (after removal of the carbonate and phosphate precipitates); because the sorbed Fe(II) comprises only a minor portion of the total Fe(II) abundance, the calculated percent oxidation is not dependent upon the efficiency of the sorbed Fe(II) extraction.

2.3. Mineral analyses and microscopy

Powder X-ray diffraction—Samples of culture suspensions were withdrawn at the end of the experiment with a syringe in an anoxic glove box and centrifuged to recover the precipitates. Remaining dissolved Fe(II) was removed from the microbially produced precipitates to avoid oxidation and formation of significant amounts of non-biogenic secondary Fe(III) precipitates through washing with water that had been degassed under vacuum, flushed with N_2 and equilibrated under an anoxic atmosphere for several days. After spreading on a glass disk, the precipitates were dried inside an anoxic glove-box. XRD spectra were obtained on a Scintag Pad V X-ray Powder Diffractometer using Cu-Kα radiation operating at 35 kV and 30 mA with a θ-2θ goniometer equipped with a germanium solid-state detector. Each scan used a 0.04° step size from 10° to 80° with a counting time of 2 seconds per step. Structures were identified by comparison to spectra in the PCPDFWIN program, © JCPDS-International Centre for Diffraction Data, 1997, (Newton Square, Pennsylvania), as well as to reference spectra obtained of synthetic ferrihydrite and goethite.

2.4. Electron microscopy

For light and scanning electron microscopy (SEM), 1 ml of a culture was taken with sterile syringes that had been flushed with N_2/CO_2. Light microscopy images of the samples were taken with a Zeiss AxioVison microscope equipped with an oil immersion objective lens. For SEM imaging, samples were chemically fixed using a half-strength Karnovsky solution, placed on holey carbon-coated EM-copper-grids, dehydrated in subsequent steps with an increasing concentration of isopropanol and finally dried in a Critical Point Dryer Bal-Tec CPD030 (for details see Schaedler et al. 2008). Dried samples were mounted on aluminium stubs using double-sided carbon tape. For enhanced electrical conductivity, the edges of the EM grids were painted with conductive silver paste. Samples which showed strong surface charging were coated in a Balzers sputter coater SCD 40 (Bal-Tec, Balzers, Liechtenstein) with a thin layer of Au/Pd (90%/10% w/w). The coating thickness was approximately 20 nm, as determined in focused ion beam cross-sections and by a surface texture analyzer (results not shown).

Imaging was performed with Zeiss Gemini 1550VP FE-SEM, Zeiss Gemini 1540XB FIB/FE-SEM, and Zeiss Ultra 55 SEM-FEG microscopes. Microscopes were equipped with Everhart-Thornley SE detectors and in-lens detectors and were optimized to a lens aperture of 30 μm. Images were recorded in a format of 1024 × 768 pixels, at integration times between 15 μs and 45 μs per pixel.

2.5. Fe isotope analyses

Iron phase separation and wet-chemical analysis—Over the course of the microbial Fe(II) oxidation experiment, subsamples were taken from each culture and abiotic control and were separated under O_2-free conditions in an anoxic glove box into solid and aqueous Fe fractions by a series of centrifugation, washing, and extraction steps as follows. At each time point, two 0.5 ml culture suspension aliquots were withdrawn in an anoxic glove box and centrifuged to separate dissolved Fe from precipitated Fe. The supernatant was separated, filtered (0.22 μm Nylon microcentrifuge tubes, Costar, Corning, NY, USA), and frozen in the closed centrifuge tubes at −18°C prior to Fe isotope analysis (see below). The remaining pellet was washed and centrifuged twice with 1 ml of anoxic water in the glovebox in order to remove loosely attached Fe leaving behind a pellet of Fe precipitates with sorbed Fe(II). The water used as wash solution for the Fe(III) precipitates contained several μM Fe(II) and about 2–4 times as much Fe(III), which probably reflects the presence of Fe(III) colloids or nano-particles in the water wash. The sorbed Fe(II) was separated for Fe isotope analysis from the pellet by extraction using a solution of 0.5 M sodium acetate (NaAc). The remaining Fe(III) pellet was frozen at −18°C until processed for Fe isotope analysis.

Iron isotope measurements—All $Fe(II)_{aq}$ and solid pellet fractions were converted to $FeCl_3$ upon repeated dry down in ambient laboratory conditions, followed by purification using anion-exchange chromatography. This procedure is identical to that used in previous biological experiments (e.g., Croal et al., 2004; Crosby et al., 2007; Wu et al., 2009), and produces accurate Fe isotope compositions regardless of the presence or absences of organics. Isotopic measurements were made using a multi-collector inductively coupled plasma mass spectrometer, as previously described (Beard et al., 2003). Data are reported as $^{56}Fe/^{54}Fe$ ratios relative to the average of igneous rocks in standard δ notation, in units of per mil (‰):

$$\delta^{56}Fe = \left[\frac{{}^{56}Fe/{}^{54}Fe_{sample}}{{}^{56}Fe/{}^{54}Fe_{IgRxs}} - 1 \right] 10^3 \quad [1]$$

$\delta^{57}Fe$ values may be defined in an analogous manner using the $^{57}Fe/^{54}Fe$ ratio. The Fe isotope fractionation between two phases or species A and B is defined as:

$$\Delta^{56}Fe_{A-B} = \delta^{56}Fe_A - \delta^{56}Fe_B \quad [2]$$

following standard practice. Measured external precision in $\delta^{56}Fe$ values is ±0.05‰ (1σ, SD) based on replicate analyses and standards. On the igneous rock scale, the $\delta^{56}Fe$ value of the IRMM-014 standard is −0.09‰ (Beard et al., 2003).

3 Results

3.1. Fe(II) oxidation and cell encrustation by the nitrate-reducing Fe(II)-oxidizing strain BoFeN1

Strain BoFeN1 oxidizes Fe(II) mixotrophically, where iron oxidation occurs with oxidation of small amounts of acetate to CO_2, coupled to the reduction of nitrate (Kappler et al., 2005). During and after Fe(II) oxidation, strain BoFeN1 becomes heavily encrusted in Fe(III) minerals (Fig. 1). In separate, but generally analogous experiments, Miot et al. (2009) demonstrated that Fe(III) minerals are present both in the periplasm as well as at the cell surface as Fe(II) oxidation proceeds; Fe(III) minerals first form in the periplasm, when no minerals are present at the cell surface. This suggests that the periplasm is the site of Fe(II) oxidation. As time passes, Fe(III) mineral precipitates in the BoFeN1 cultures associate with extracellular filaments (Fig. 1),

which Miot et al. (2009) identified as polysaccharides. This contrasts with the studies of Straub et al. (1996) and Schaedler et al. (2008), who showed that another nitrate-reducing, autotrophic Fe(II)-oxidizing (enrichment) culture contained only cells that are not encrusted but associated with Fe(III) minerals.

Analysis of the Fe(III) solids by XRD produced no strong signal (not shown), indicating that the Fe(III) minerals produced were either amorphous or very finely crystalline. EDX spectra showed only Fe and O peaks, indicating that no significant quantities of Fe phosphates were formed as were found in the experiments of Miot et al. (2009). This is consistent with the relatively low phosphate contents of the medium used in the current study (approximately 40 μM after filtration of the Fe(II)-carbonates and Fe(II)-phosphates formed upon $Fe(II)Cl_2$ addition to the medium). The absence of carbonates in STXM analysis of the experiments of Miot et al. (2009) also suggests that during the co-metabolic acetate oxidation and CO_2 production, no Fe(II) carbonates precipitated during the course of Fe(II) oxidation. The products of Fe(II) oxidation in the current study, run at 16 °C and 30 °C, are similar to those observed by Kappler et al. (2005), who studied Fe(II) oxidation by strain BoFeN1 at 30 °C in cultures that were inoculated with cells that were pre-grown using acetate/nitrate and Fe(II)/acetate/nitrate. In the acetate/nitrate cultures, Kappler et al. (2005) determined a BET surface area of 158 $m^2\ g^{-1}$ for the Fe(III) products and found no XRD signals, suggesting a mixture of ferrihydrite and nano-crystalline goethite, whereas the Fe(II)/acetate/nitrate cultures produced clear evidence of nano-crystalline goethite, based on XRD spectra. Mössbauer spectroscopy of Fe(III) solids produced by acetate/nitrate BoFeN1 cultures in experiments similar to the current study suggests a mixture of nano-crystalline goethite and/or ferrihydrite (Hohmann et al., 2010). We conclude that the Fe(III) minerals produced in our experiments likely consisted of large amounts of ferrihydrite and/or nano-crystalline goethite. If the products were mixtures of ferrihydrite and/or nano-crystalline goethite, it is likely that the proportions of these minerals change over time; based on the results of Kappler et al. (2005) and Hohmann et al. (2010), we would expect the proportion of nano-crystalline goethite to be higher in the later time points, where the probability of phase conversion of poorly crystalline Fe(III) hydroxides would be greatest. In the present study, we will use "$Fe(OH)_3$" in a generic sense to describe a variety of poorly crystalline ferric hydroxides such as ferrihydrite, as well as minerals such as schwertmannite and akaganeite, which were produced in some of the experiments of Balci et al. (2006).

In the present study, we observed that approximately 80% of the Fe(II) initially present was oxidized by strain BoFeN1 at 16°C by 21 days (Fig. 2). The average oxidation rates in the strain BoFeN1 experiments at 16°C lie between those observed by Croal et al. (2004) for phototrophic Fe(II) oxidation at 40 and 80 cm light distances (40W light source) at room temperature, but significantly higher than the rates observed at 120 cm light distances by Croal et al. (2004) (Fig. 3). The average oxidation rates observed in the 16 °C strain BoFeN1 experiments were much higher than those observed by Balci et al. (2006) in their low-pH bacterial Fe(II) oxidation experiments. The average oxidation rates of the 30°C strain BoFeN1 experiments were very fast, where complete oxidation occurred within 4 days (Fig. 2 and 3). Sorbed Fe(II) contents for the 16 °C experiments increased in the first five days and then levelled off (Fig. 2), suggesting no major changes in the sorption capacity of the Fe(III) minerals. In contrast, sorbed Fe(II) contents in the 30 °C experiments increased dramatically in the first few days, where oxidation rates were very fast, but decreased after 3 days, levelling off to the end of the experiment (Fig. 2); this may suggest a decrease in surface area of the Fe (III) minerals, possibly reflecting conversion to larger crystals, or conversion of ferrihydrite to crystalline ferric hydroxides such as goethite. Additionally, decreasing $Fe(II)_{sorb}$ contents can be a result of the depletion of Fe(II) in solution.

3.2. Fe isotope fractionation by the nitrate-reducing Fe(II)-oxidizing strain BoFeN1

The $\delta^{56}Fe$ values for $Fe(II)_{aq}$ and the $Fe(OH)_3$ precipitate produced in the strain BoFeN1 experiments varied systematically as a function of fraction oxidized (Fig. 4). As is the case with all biological or abiological Fe(II) oxidation experiments to date, the isotopic variations may be described by two end-member models, one involving continuous isotopic equilibrium in a closed system, and one involving Rayleigh fractionation using a kinetic or equilibrium fractionation factor but where the solid is prevented from re-equilibrating with $Fe(II)_{aq}$ after precipitation (e.g., Bullen et al., 2001;Beard and Johnson, 2004;Johnson et al., 2004a;Croal et al., 2004;Balci et al., 2006; Dauphas and Roxell, 2006). The $\delta^{56}Fe$ values for the $Fe(OH)_3$ precipitate at low fraction oxidized scatter between a trend described by Rayleigh fractionation using a $\Delta^{56}Fe_{Fe(OH)3 - Fe(II)aq}$ fractionation factor of +1.5 to 2.0 ‰ (solid black curve in Fig. 4 shown for +2.0 ‰ fractionation) and a trend that accounts for partial isotopere-equilibration between $Fe(OH)_3$ and $Fe(II)_{aq}$. Partial isotopic re-equilibration of the precipitate was modeled using the mass-balance equations of Crosby et al. (2007), assuming precipitates that initially formed through Rayleigh fractionation ($\Delta^{56}Fe_{Fe(OH)3 - Fe(II)aq}$ = +2.0 ‰) maintained isotopic equilibrium between a 1 nm-thick reactive Fe(III) layer on the surface of a 10 nm-diameter spherical precipitate, sorbed Fe(II), and aqueous Fe(II) (see Fig. 4 caption for details); if the thickness of the reactive Fe(III) layer is increased, or the dimensions of the particle changes such that the ratio of surface atoms to total atoms increases (e.g., rod-shaped goethite), the partial re-equilibration model will move toward a closed-system equilibrium model (solid diagonal grey lines in Fig. 4). In contrast, for the data for the 16 °C experiments, the $\delta^{56}Fe$ values for the $Fe(OH)_3$ precipitate follow a closed-system equilibrium trend after ~30 % oxidation using an equilibrium $\Delta^{56}Fe_{Fe(OH)3 - Fe(II)aq}$ fractionation factor of +3.0 ‰ (Fig. 4). From 0 to 40 % oxidation, the $\delta^{56}Fe$ values for the $Fe(OH)_3$ precipitate in the 30 °C experiments appear to be better described by a Rayleigh fractionation process (Fig. 4), which would be more likely at the higher oxidation and precipitation rates of the higher temperature experiments.

The $\delta^{56}Fe$ values for $Fe(II)_{aq}$ from 0 to 60% oxidized decrease with progressive oxidation, but, as noted by Croal et al. (2004), at low extents of oxidation the isotopic composition of Fe $(II)_{aq}$ during oxidation is not sensitive to a particular fractionation model such as Rayleigh or equilibrium fractionation (Fig. 4). We stress that the Rayleigh models shown in Fig. 4 are primarily for illustrating potential processes that may explain the isotopic data, and a variety of $Fe(OH)_3 - Fe(II)_{aq}$ fractionation factors between +1 and +3 ‰ may describe the results at the early stages of oxidation where the scatter is greatest for any particular time point. The $\delta^{56}Fe$ values for $Fe(II)_{aq}$ in the 16 °C experiments at ~80 % oxidation appear to be anomalously high, relative to any fractionation model that fits the data at smaller degrees of oxidation. Although it is possible that anomalously high $\delta^{56}Fe$ values for $Fe(II)_{aq}$ could be produced by contamination by $Fe(OH)_3$ precipitates, great care was taken to ensure complete separation of solid and aqueous components. The $\delta^{56}Fe$ values for $Fe(II)_{aq}$ in the 30°C experiments at complete- or near-complete oxidation lie between those expected for a Rayleigh or equilibrium fractionation trend (Fig. 4).

4 Discussion

The new results presented here for strain BoFeN1, when combined with previous studies of Fe isotope fractionation by Croal et al. (2004) and Balci et al. (2006), provide a broad view of Fe isotope fractionation during biological Fe(II) oxidation via a variety of pathways that utilize different electron acceptors. Important issues arising from these studies include the measured or inferred abundance of aqueous Fe(III), the degree of isotopic equilibrium between Fe $(II)_{aq}$ and ferric hydroxide precipitates, and kinetic isotope effects upon precipitation.

4.1. Fe isotope fractionation by chemical and biological Fe(II) oxidation

In all cases of biological Fe(II) oxidation, ferric hydroxide precipitates have higher $\delta^{56}Fe$ values than coexisting $Fe(II)_{aq}$ (Fig. 5), consistent with the expected relative fractionation based on experimental (Johnson et al., 2002;Skulan et al., 2002;Welch et al., 2003) and theoretical (Polyakov and Mineev, 2000;Schauble et al., 2001) studies. The degree of fractionation between $Fe(OH)_3$ and $Fe(II)_{aq}$ among these studies, however, is variable. Relative to the results obtained here, the fractionation between $Fe(OH)_3$ and $Fe(II)_{aq}$ measured for phototrophic Fe (II) oxidation (Croal et al., 2004) is significantly less (Fig. 5A). Microbial oxidation of Fe(II) at low-pH (Balci et al., 2006) produced a wide range of $\delta^{56}Fe$ values for $Fe(OH)_3$, overlapping with the range measured in this study, but also producing higher and lower $\delta^{56}Fe$ values (Figs. 5B and 5C). In addition, microbial oxidation of Fe(II) at low pH produces significant quantities of $Fe(III)_{aq}$, and Balci et al. (2006) noted that the $\delta^{56}Fe$ values for $Fe(III)_{aq}$ were always greater than those of co-existing $Fe(II)_{aq}$ (Figs. 5B and 5C), as expected from abiological experiments and theoretical predictions.

In Figure 6 we compare the $\Delta^{56}Fe_{Fe(OH)3 - Fe(II)aq}$ fractionations measured in the current study (Fig. 6A), with those determined for phototrophic Fe(II) oxidation (Fig. 6B), and low-pH Fe (II) oxidation (Fig. 6C), as well as the $\Delta^{56}Fe_{Fe(III)aq - Fe(II)aq}$ fractionations measured for low-pH microbial oxidation where significant quantities of $Fe(III)_{aq}$ were produced (Fig. 6D). As initially proposed by Beard and Johnson (2004) and Johnson et al. (2004b), and expanded upon by Dauphas and Rouxell (2006), the overall fractionation between $Fe(OH)_3$ precipitate and Fe $(II)_{aq}$ during Fe(II) oxidation can be approximated by the relation:

$$\Delta^{56}Fe_{Fe(OH)3-Fe(II)aq} \approx \Delta^{56}Fe_{Fe(III)aq-Fe(II)aq} + \Delta^{56}Fe_{Fe(OH)3-Fe(III)aq} \quad [3]$$

if $Fe(III)_{aq}$ is present as an intermediate component; this approximation is valid where the proportion of $Fe(III)_{aq}$ is ≤5% of the total aqueous Fe. At larger proportions of $Fe(III)_{aq}$, such as the experiments of Balci et al. (2006), the overall $Fe(OH)_3 - Fe(II)_{aq}$ fractionation may deviate from equation 3 by up to ~1 ‰, producing a smaller net $Fe(OH)_3 - Fe(II)_{aq}$ fractionation for a given set of values for $\Delta^{56}Fe_{Fe(III)aq - Fe(II)aq}$ and $\Delta^{56}Fe_{Fe(OH)3 - Fe(III)aq}$ (Beard and Johnson, 2004).

The measured $\Delta^{56}Fe_{Fe(OH)3 - Fe(II)aq}$ fractionations during the initial stages of oxidation for strain BoFeN1 are consistent with a Rayleigh trend using an overall $\Delta^{56}Fe_{Fe(OH)3 - Fe(II)aq}$ fractionation factor of ~+2.0 ‰, as well as possible partial isotopic re-equilibration (Fig. 6A), which we interpret to reflect initial precipitation that combines an equilibrium $\Delta^{56}Fe_{Fe(III)aq - Fe(II)aq}$ fractionation of ~+3.0 ‰ and a kinetic $\Delta^{56}Fe_{Fe(OH)3 - Fe(III)aq}$ fractionation of ~ −1.0 ‰, assuming a two-step oxidation and precipitation model (Beard and Johnson, 2004). It is certainly possible that different net $Fe(OH)_3 - Fe(II)_{aq}$ fractionation factors may be chosen to explain different time points at <20% oxidation, consistent with the overall conclusion that a combination of equilibrium $Fe(III)_{aq} - Fe(II)_{aq}$ fractionation, but variable kinetic $Fe(OH)_3 - Fe(III)_{aq}$ fractionation, is responsible for the observed net Fe $(OH)_3 - Fe(II)_{aq}$ fractionations for the early time points. Between ~20 and 60 % oxidation, however, the overall $\Delta^{56}Fe_{Fe(OH)3 - Fe(II)aq}$ fractionation appears to lie along a fractionation line of +3.0 ‰, which could reflect an equilibrium fractionation factor, assuming a near-zero $\Delta^{56}Fe_{Fe(OH)3 - Fe(III)aq}$ fractionation factor; the $Fe(OH)_3 - Fe(III)_{aq}$ fractionation factor has not been measured experimentally, nor predicted from theory, and possible values for this fractionation factor are discussed in the next section. At ~60–80 % oxidation, the $Fe(OH)_3 - Fe(II)_{aq}$ fractionation at 16 °C decreases to ~ +2.2 ‰, and this is caused by an increase in the $\delta^{56}Fe$ value for $Fe(II)_{aq}$ relative to that predicted by a Rayleigh fractionation or closed-system equilibrium relation at a constant fractionation factor (Fig. 4), possibly reflecting a change in

the nature of the Fe(III) precipitate (from ferrihydrite to goethite, see above, or potential changes in crystallinity of the formed ferrihydrite and goethite). The +3 to +4 ‰ $\Delta^{56}Fe_{Fe(OH)3 - Fe(II)aq}$ fractionation at the end of the 30 °C experiment may be explained in part by a Rayleigh process, which produces high fractionations when $Fe(II)_{aq}$ contents become very small (Fig. 6).

The overall $\Delta^{56}Fe_{Fe(OH)3 - Fe(II)aq}$ fractionation measured for phototrophic Fe(II) oxidation (Fig. 6B) is generally less than that measured for strain BoFeN1 (current study). Croal et al. (2004) noted that the relatively small fractionation measured for phototrophic Fe(II) oxidation may reflect 1) a unique equilibrium Fe isotope fractionation via binding to biological ligands, and/or 2) a two-step fractionation involving an equilibrium $Fe(III)_{aq} - Fe(II)_{aq}$ fractionation combined with a kinetic $Fe(OH)_3 - Fe(III)_{aq}$ fractionation upon precipitation; subsequent studies have demonstrated the importance of a two-step, equilibrium-kinetic process associated with abiological Fe(II) oxidation (Beard and Johnson, 2004;Johnson et al., 2004b), and we therefore prefer the second interpretation for the $\Delta^{56}Fe_{Fe(OH)3 - Fe(II)aq}$ fractionations observed by Croal et al. (2004). Although there was no measurable ambient $Fe(III)_{aq}$ in the experiments of Croal et al. (2004), it is possible that local decreases in pH at the cell interface allowed $Fe(III)_{aq}$ to exist (Kappler and Newman, 2004), which would permit a two-step oxidation mechanism. Additionally, the existence of an intracellular ligand that controls the $Fe(III)_{aq}$ pool cannot yet be excluded.

A range in overall $\Delta^{56}Fe_{Fe(OH)3 - Fe(II)aq}$ fractionations was measured by Balci et al. (2006) during low-pH microbial Fe(II) oxidation (Fig. 6C). As noted by Balci et al. (2006), the net $Fe(OH)_3 - Fe(II)_{aq}$ fractionation probably reflects a significant $Fe(OH)_3 - Fe(III)_{aq}$ fractionation upon precipitation, in addition to $Fe(III)_{aq} - Fe(II)_{aq}$ fractionation, which will decrease the net $Fe(OH)_3 - Fe(II)_{aq}$ fractionation if the $\Delta^{56}Fe_{Fe(OH)3 - Fe(III)aq}$ fractionation factor is negative. Based on regression of Fe isotope data for $Fe(II)_{aq}$, Balci et al. (2006) inferred a net $Fe(OH)_3 - Fe(II)_{aq}$ fractionation of +2.2 ‰. Balci et al. (2006) noted that, based on direct measurement of $Fe(III)_{aq}$ and $Fe(II)_{aq}$, their results were broadly consistent with the equilibrium $Fe(III)_{aq} - Fe(II)_{aq}$ fractionation of +3.0 ‰ measured in abiologic experiments and predicted by theory (e.g., Anbar et al., 2005; Domagal-Goldman and Kubicki, 2008; Johnson et al., 2002; Welch et al., 2003).

4.2. The effects of kinetic fractionations upon precipitation

We suggest that any variations in the measured overall $Fe(OH)_3 - Fe(II)_{aq}$ fractionation must reflect variable kinetic effects on the $Fe(OH)_3 - Fe(III)_{aq}$ fractionation upon precipitation. As noted in Section 2.1, the effects of aqueous speciation on the Fe isotope fractionations will be small in the experiments, <0.1 ‰ in $^{56}Fe/^{54}Fe$. Based on the temperature dependence determined by Welch et al. (2003), Anbar et al. (2005), and Domagal-Goldman and Kubicki (2008), the $Fe(III)_{aq} - Fe(II)_{aq}$ fractionation should be ~0.3 ‰ less at 30 °C than it is at 16 °C. We have compiled the data available for ferric oxide/hydroxide – $Fe(III)_{aq}$ fractionations in Figure 7, drawing from the studies of Skulan et al. (2002) and Balci et al. (2006). There have been no studies that have determined the equilibrium fractionation between ferrihydrite and $Fe(III)_{aq}$, because even for nm-size crystals, isotopic exchange between these components is limited to surface atom sites (Poulson et al., 2005). The equilibrium fractionation between hematite and $Fe(III)_{aq}$ has been estimated by Skulan et al. (2002) based on experiments that underwent >80 % exchange (determined by ^{57}Fe-enriched tracer studies). These experiments, however, were run at temperatures above the stability range for goethite, and therefore extrapolation to room temperatures requires some assumptions. Nevertheless, the equilibrium $Fe_2O_3 - Fe(III)_{aq}$ fractionation at room temperature is estimated to lie between 0.0 and +0.4 ‰ (Fig. 7). Skulan et al. (2002) measured a kinetic $Fe_2O_3 - Fe(III)_{aq}$ fractionation between −1.0 and −1.5 ‰ that approximately followed a Rayleigh process (Fig. 7).

Balci et al. (2006) investigated the fractionation between ferric hydroxide precipitates and Fe(III)$_{aq}$ in a range of abiologic and biologic experiments, and in almost all cases found a negative fractionation (Fig. 7), which can also be observed in Figures 5B and 5C through comparison of data for the precipitate and Fe(III)$_{aq}$. The differences in Fe(OH)$_3$ - Fe(III)$_{aq}$ fractionation for ferric chloride and ferric sulfate observed by Balci et al. (2006) (Fig. 7) may in part reflect differences in the precipitate that was produced, where ferric sulfate solutions produced schwertmannite and ferric chloride solutions produced akaganeite. As noted by Balci et al. (2006), it is difficult at this time to infer the equilibrium Fe(OH)$_3$ – Fe(III)$_{aq}$ fractionation factor. If we assume that the equilibrium Fe(OH)$_3$ – Fe(III)$_{aq}$ fractionation is approximately equal to the equilibrium Fe_2O_3 – Fe(III)$_{aq}$ fractionation, then the negative Fe(OH)$_3$ – Fe(III)$_{aq}$ fractionations in Figure 7 may reflect kinetic effects. We suggest that the equilibrium Fe(OH)$_3$ – Fe(III)$_{aq}$ fractionation factor is probably close to zero, but it is important to stress that this fractionation factor is not well constrained by experiments, nor has it been calculated from theory.

4.3. Implications for biological Fe(II) oxidation mechanisms

The observation that the Fe(OH)$_3$ – Fe(II)$_{aq}$ isotope fractionations during oxidation of Fe(II)$_{aq}$ by strain BoFeN1 approach those expected for equilibrium conditions between ~20 and 60 % oxidation (Fig. 6A) suggests that the oxidation pathway must permit redox cycling between Fe(OH)$_3$ and Fe(II)$_{aq}$. Fig. 8A shows the three different locations where Fe(OH)$_3$ precipitation was observed after oxidation of Fe(II)$_{aq}$ by strain BoFeN1 (Miot et al., 2009), i.e. in the periplasm, at the cell surface or at a distance to the cells (e.g. at exopolysaccharides). The proportion of oxides that is formed in the periplasm versus the fraction of mineral that is formed extracellularly is unknown. As discussed above, unidirectional oxidation of Fe(II)$_{aq}$ to Fe(III)$_{aq}$, followed by precipitation of Fe(III)$_{aq}$ to Fe(OH)$_3$, tends to produce overall Fe(OH)$_3$ – Fe(II)$_{aq}$ isotope fractionations that are less than those expected for equilibrium conditions, and this probably reflects the very low rates of isotopic exchange between Fe(III)$_{aq}$ and Fe(III) oxides or hydroxides. For example, Poulson et al. (2005) noted that only ~26 % isotopic exchange occurred between Fe(III)$_{aq}$ and 3 nm-size ferrihydrite in 10 days at room temperature, with little subsequent exchange up to the end of the 85 day experiment. Skulan et al. (2002) noted that 150 days were required to attain ~80 % isotopic exchange between Fe(III)$_{aq}$ and 200 nm-size hematite at 98 °C. In contrast, Handler et al. (2009) noted that 100 % isotopic exchange occurred between Fe(II)$_{aq}$ and 100 nm-long goethite at room temperature within ~15 days. These observations suggest that equilibrium Fe isotope fractionation upon Fe(II) oxidation will most likely be attained when Fe(II)$_{aq}$ and Fe(III) oxide/hydroxides remain in close contact, with low Fe(III)$_{aq}$ contents, to permit a continuous state of coupled Fe atom and electron exchange between Fe(II)$_{aq}$ and Fe(III) precipitates. High Fe(III)$_{aq}$ contents would be expected to inhibit aqueous-oxide isotopic exchange.

Unidirectional oxidation of Fe(II)$_{aq}$ to Fe(III)$_{aq}$, and attendant equilibrium isotope fractionation, followed by quantitative precipitation to Fe(OH)$_3$ with no fractionation, is an alternative pathway that would reflect equilibrium conditions among aqueous species but no isotopic exchange between aqueous Fe and Fe(OH)$_3$. Such a pathway is modeled using a Rayleigh process with a net Fe(OH)$_3$-Fe(II)$_{aq}$ fractionation factor of +3 ‰ for $^{56}Fe/^{54}Fe$ (Figs. 6A–6C). It is clear, however, that such a process does not fit the observed data, and, in particular, cannot explain the ~+3 ‰ Fe(OH)$_3$ – Fe(II)$_{aq}$ fractionations at intermediate stages of oxidation. We therefore conclude that Fe(II)$_{aq}$ – Fe(OH)$_3$ redox cycling is the best explanation for the observed isotopic fractionations.

In their study of Fe(II) oxidation by strain BoFeN1, Miot et al. (2009) concluded that Fe(II) oxidation began in the periplasm, producing Fe(III) precipitates that resulted in cell encrustation. An important finding in the study by Miot et al. was the observation that a

consistent Fe(II)/Fe(III) precipitate ratio existed in the periplasm of the cells at any given time, independent of the degree of encrustation of individual cells, suggesting a continual state of redox equilibrium between the periplasm and the ambient conditions in the culture. Miot et al. (2009) concluded that active Fe(II) – Fe(III) redox cycling occurred in the periplasm during Fe(II) oxidation by strain BoFeN1. This suggests that Fe isotope equilibrium is likely to be maintained between $Fe(II)_{aq}$ and Fe(III) precipitates in the periplasm (for illustration see Fig. 8B), consistent with the ~3 ‰ $Fe(OH)_3$ – $Fe(II)_{aq}$ isotope fractionation measured for samples that reflect ~20 to 60 % oxidation in the 16 °C experiments; as noted above, the lower fractionations at <20 % oxidation are interpreted to reflect kinetic effects during the early stages of Fe(II) oxidation, when the rates of oxidation were highest. Isotopic equilibration through redox cycling is expected to be less effective outside the periplasm (Fig. 8C) because the large quantities of clumped $Fe(OH)_3$ aggregates observed outside the cells (Miot et al., 2009; Schaedler et al., 2009) will be less likely to undergo isotopic exchange with aqueous Fe, as compared to the restricted environment of the periplasm where smaller $Fe(OH)_3$ particles with high surface-per volume ratios are present (Miot et al., 2009). We conclude that microbial Fe (II) oxidation that involves oxidation *and* Fe(III) mineral precipitation in the periplasm is most likely to produce an equilibrium Fe isotope fractionation relative to Fe(III) mineral precipitation that occurs extracellularly, as in the studies of Croal et al. (2004) and Balci et al. (2006). It should be noted, however, that the scenarios presented in Fig. 8B and C reflect two extremes of either periplasmic or extracellular $Fe(OH)_3$ precipitation following periplasmic Fe(II) oxidation. In reality the process will probably reflect a combination of these scenarios at different time points of Fe(II) oxidation. As a consequence, in future experiments the proportion of Fe(III) oxides that forms in the periplasm of BoFeN1 relative to the total amount of Fe(III) oxides present should be determined during the course of Fe(II) oxidation.

We speculate that the decrease in $Fe(OH)_3$ – $Fe(II)_{aq}$ fractionation at ~80 % oxidation in the 16 °C experiments reflects an increase in the proportion of well-crystallized goethite in the Fe (III) precipitates. Polyakov and Mineev (2000) predicted that the $\delta^{56}Fe$ values of goethite should be 2.1 ‰ lower than those of hematite at room temperature, which would decrease the Fe(III) oxide/hydroxide – $Fe(II)_{aq}$ fractionation to ~ +1 ‰. If well-crystallized goethite preferentially exchanged with the remaining $Fe(II)_{aq}$ at ~80 % oxidation via a Fe(II)-promoted phase transformation, the overall Fe(III) precipitate – $Fe(II)_{aq}$ isotope fractionation would decrease, as observed (Fig. 6A).

Alternatively, the decrease in $Fe(OH)_3$ – $Fe(II)_{aq}$ fractionation at ~80 % oxidation in the 16 ° C experiments could indicate that some Fe(II) is oxidized chemically (and extracellularly) by nitrite without reaching the 3 per mil equilibrium fractionation. Such a contribution of abiotic Fe(II) oxidation was suggested to occur at the end of the Fe(II) oxidation in BoFeN1 cultures by Kappler et al. (2005) and Miot et al. (2009). Additional uncertainties exist for the 30 °C experiments because the fast oxidation and precipitation kinetics would make it less likely to produce equilibrium isotopic fractionations.

5. Conclusions

Microbial Fe(II) oxidation coupled to reduction of CO_2, O_2, or NO_3^- consistently produces positive Fe isotope fractionations between Fe(III) oxide/hydroxide precipitates and aqueous Fe(II). In many cases, the measured $Fe(OH)_3$ – $Fe(II)_{aq}$ fractionations at low extent of oxidation, where fractionations are not strongly dependent upon closed-system equilibrium or Rayleigh models, are less than the ~ +3 ‰ fractionation estimated to reflect equilibrium conditions at room temperature. Based on the rapid rates of isotopic exchange between Fe $(II)_{aq}$ and Fe(III) oxide/hydroxide (Handler et al., 2009), relative to the slow rates of exchange for $Fe(III)_{aq}$, (Poulson et al., 2005; Skulan et al., 2002), we propose that equilibrium Fe isotope fractionation during biological Fe(II) oxidation is most likely to be produced under conditions

of continuous electron and atom exchange, in environments that promote redox cycling. These conditions may be satisfied when Fe(II) oxidation and initial Fe(III) mineral precipitation occur in the periplasm, as they do for *Acidovorax* sp. strain BoFeN1. We hypothesize that the isotopic fractionations produced by biological oxidation pathways that involve initial Fe(III) mineral precipitation outside the cell, such as the neutrophilic phototroph *Thiodictyon* sp. (Croal et al., 2004), or the acidophilic Fe(II) oxidizer *Acidothiobacilus* sp. (Balci et al., 2006), or abiological oxidation of $Fe(II)_{aq}$ (Bullen et al., 2001), are unlikely to reflect equilibrium conditions because Fe(II) – Fe(III) oxide/hydroxide redox cycling may be inhibited where significant quantities of $Fe(III)_{aq}$ exist, or where much larger quantities of Fe(III) precipitates exist in the ambient environment. Determining the proportion of Fe(III) oxides that first form in the periplasm of BoFeN1, relative to the total amount of Fe(III) oxides that eventually encrust the cell, is a priority for future research.

Although uncertainties remain with regard to the equilibrium $Fe(OH)_3$ – $Fe(II)_{aq}$ isotope fractionation factor, which is important for comparison to biological Fe(II) oxidation, the results of the current study demonstrate that distinct Fe isotope fractionations may be produced by different oxidative pathways. The rapid rates of isotopic exchange between $Fe(II)_{aq}$ and $Fe(III)_{aq}$ suggests that these species should always be in isotopic equilibrium even under conditions of very rapid Fe(II) oxidation. The isotopic effects of sorption are difficult to estimate for experiments that produced ferrihydrite because the equilibrium $Fe(II)_{sorb}$ – $Fe(II)_{aq}$ fractionation has not been determined for ferrihydrite substrates. Under conditions of isotopic equilibrium, however, fractionations between aqueous and sorbed Fe(II) will not affect the overall $Fe(OH)_3$ – $Fe(II)_{aq}$ fractionation. Kinetic fractionation upon precipitation of $Fe(OH)_3$, therefore, is the most likely explanation for measured $Fe(OH)_3$ – $Fe(II)_{aq}$ fractionations at low extent of oxidation that are less than ~ +3 ‰.

Acknowledgments

The research was supported by a post-doc fellowship and an Emmy-Noether fellowship from the German Research Foundation (DFG) to AK and a grant from the Packard Foundation to DKN. Additional funding from the NASA Astrobiology Institute supported CMJ and BLB, and funding from the National Science Foundation supported BLB and HAC. We would like to thank Ma Chi (Caltech) for help with the XRD. Sebastian Schaedler (University of Tuebingen) and Claus Burkhardt (NMI Reutlingen) are acknowledged for providing scanning electron micrographs. DKN is an Investigator of the Howard Hughes Medical Institute. We thank AE Stephan Kraemer, Thomas Bullen, and an anonymous reviewer, whose comments helped improve the manuscript.

References

Anbar AD, Jarzecki AA, Spiro TG. Theoretical investigation of iron isotope fractionation between $Fe(H_2O)_6^{3+}$ and $Fe(H_2O)_6^{2+}$: Implications for iron stable isotope geochemistry. Geochim Cosmochim Acta 2005;69:825–837.

Anbar AD. Iron stable isotopes: beyond biosignatures. Earth Planet Sci Lett 2004;217:223–236.

Balci N, Bullen TD, Witte-Lien K, Shanks WC, Motelica M, Mandernack KW. Iron isotope fractionation during microbially stimulated Fe(II) oxidation and Fe(III) precipitation. Geochim Cosmochim Acta 2006;70:622–639.

Beard BL, Johnson CM, Cox L, Sun H, Nealson KH, Aguilar C. Iron isotope biosignatures. Science 1999;285:1889–1892. [PubMed: 10489362]

Beard BL, Johnson CM, Skulan JL, Nealson KH, Cox L, Sun H. Application of Fe isotopes to tracing the geochemical and biological cycling of Fe. Special issue on Isotopic Record of Microbially Mediated Processes. Chem Geol 2003;195:87–117.

Beard BL, Johnson CM. Fe isotope variations in the modern and ancient earth and other planetary bodies. Geochemistry of Non-Traditional Stable Isotopes 2004;55:319–357.

Bullen TD, White AF, Childs CW, Vivit DV, Schulz MS. Demonstration of significant abiotic iron isotope fractionation in nature. Geology 2001;29:699–702.

Cornell, RM.; Schwertmann, U. The iron oxides: structure, properties, reactions, occurrences and uses. Wiley-VCH Verlag GmbH & Co; Weinheim, Germany: 2003.

Croal LR, Johnson CM, Beard BL, Newman DK. Iron isotope fractionation by Fe(II)-oxidizing photoautotrophic bacteria. Geochim Cosmochim Acta 2004;68 (6):1227–1242.

Croal LR, Jiao Y, Newman DK. The fox operon from *Rhodobacter* strain SW2 promotes phototrophic Fe(II) oxidation in *Rhodobacter capsulatus* SB1003. J Bacteriol 2007;189:1774–1782. [PubMed: 17189371]

Crosby HA, Roden EE, Johnson CM, Beard BL. The mechanisms of iron isotope fractionation produced during dissimilatory Fe(III) reduction by *Shewanella putrefaciens* and *Geobacter sulfurreducens*. Geobiology 2007;5:169–189.

Dideriksen K, Baker JA, Stipp SLS. Equilibrium Fe isotope fractionation between inorganic aqueous Fe (III) and the siderophore complex Fe(III)-desferrioxamine B. Earth Planet Sci Lett 2008;269:280–290.

Domagal-Goldman SD, Kubicki JD. Density functional theory predictions of equilibrium isotope fractionation of iron redox changes and organic complexation. Geochim Cosmochim Acta 2008;72:5201–5216.

Ehrenreich A, Widdel F. Anaerobic oxidation of ferrous iron by purple bacteria, a new-type of phototrophic metabolism. Appl Envrion Microbiol 1994;60:4517–4526.

Ehrlich, HL.; Newman, DK. Geomicrobiology. 5. CRC Press; 2008. p. 656

Emerson D, Moyer C. Isolation and characterization of novel iron-oxidizing bacteria that grow at circumneutral pH. Appl Environ Microbiology 1997;63(12):4784–4792.

Emerson D, Revsbech NP. Investigation of an iron-oxidizing microbial mat community located near Aarhus, Denmark: Field studies. Appl Environ Microbiology 1994;60(11):4022–4031.

Farquhar J, Wing BA. Multiple sulfur isotopes and the evolution of the atmosphere. Earth Planet Sci Lett 2003;213:1–13.

Hafenbradl D, Keller M, Dirmeier R, Rachel R, Rossnagel P, Burggraf S, Huber H, Stetter KO. *Ferroglobus placidus* gen. nov., sp Nov., a novel hyperthermophilic archeum that oxidizes Fe^{2+} at neutral pH under anoxic conditions. Arch Microbiol 1996;166:308–314. [PubMed: 8929276]

Handler RM, Beard BL, Johnson CM, Scherer MM. Atom exchange between aqueous Fe(II) and goethite: an Fe isotope tracer study. Environ Sci & Technol 2009;43:1102–1107. [PubMed: 19320165]

Hanert, HH. The genus *Gallionella*. In: Starr, MP.; Stolp, H.; Trueper, HG.; Balows, A.; Schlegel, HG., editors. The Prokaryotes. Springer; Berlin: 1981. p. 509-515.

Hegler F, Posth NR, Jiang J, Kappler A. Physiology of phototrophic iron(II)-oxidizing bacteria – implications for modern and ancient environments. FEMS Microbiol Ecol 2008;66:250–260. [PubMed: 18811650]

Hill PS, Schauble EA. Modeling the effects of bond environment on equilibrium iron isotope fractionation in ferric aquo-chloro complexes. Geochimica et Cosmochimica Acta 2008;72:1939–1958.

Hohmann C, Winkler E, Morin G, Kappler A. Anaerobic Fe(II)-oxidizing bacteria show As resistance and co-precipitate As during Fe(III) mineral precipitation. Environmental Science and Technology 2010;44:94–101. [PubMed: 20039738]

Jeon B, Dempsey BA, Burgos WD, Royer RA, Roden EE. Modeling the sorption kinetics of divalent metal ions to hematite. Water Research 2004;38(10):2499–2504. [PubMed: 15159153]

Jiao Y, Kappler A, Croal LR, Newman DK. Isolation and characterization of a genetically traceable photoautotrophic Fe(II)-oxidizing bacterium, *Rhodopseudomonas palustris* strain TIE-1. Appl Environ Microbiol 2005;71:4487–4496. [PubMed: 16085840]

Jiao Y, Newman DK. The pio operon is essential for phototrophic Fe(II) oxidation in *Rhodopseudomonas palustris* TIE-1. J Bacteriol 2007;189:1765–1773. [PubMed: 17189359]

Johnson C, Beard B, Albarede F. Geochemistry of non-traditional stable isotopes - Overview and General Concepts. Rev Mineral Geochem Geochemistry of Non-Traditional Stable Isotopes 2004a;55

Johnson CM, Beard BL, Roden EE, Newman DK, Nealson KH. Isotopic constraints on biogeochemical cycling of Fe. Rev Mineral Geochem Geochemistry of Non-Traditional Stable Isotopes 2004b; 55:359–408.

Johnson CM, Skulan JL, Beard BL, Sun H, Nealson KH, Braterman PS. Isotopic fractionation between Fe(III) and Fe(II) in aqueous solutions. Earth Planet Sci Lett 2002;195(1–2):141–153.

Johnson CM, Skulan JL, Beard BL, Sun H, Nealson KH, Braterman PS. Isotopic fractionation between Fe(III) and Fe(II) in aqueous solutions. Earth Planet Sci Lett 2002;195:141–153.

Kappler A, Newman DK. Formation of Fe(III)-minerals by Fe(II)-oxidizing phototrophic bacteria. Geochim Cosmochim Acta 2004;68:1217–1226.

Kappler A, Straub KL. Geomicrobiological cycling of iron. Rev Mineral Geochem 2005;59:85–108.

Kappler A, Schink B, Newman DK. Fe(III) mineral formation and cell encrustation by the nitrate-dependent Fe(II)-oxidizer strain BoFeN1. Geobiology 2005;3:235–245.

Lovley DR, Holmes DE, Nevin KP. Dissimilatory Fe(III) and Mn(IV) reduction. Adv Microbial Physiol 2004;49:219–286.

Miot J, Benzerara K, Morin M, Kappler A, Bernard S, Obst M, Férard F, Skouri-Panet F, Guigner JM, Posth N, Galvez M, Brown GE Jr, Guyot F. Iron biomineralization by neutrophilic iron-oxidizing bacteria. Geochim Cosmochim Acta 2009;73:696–711.

Neubauer, SC.; Emerson, D.; Megonigal, JP. Microbial oxidation and reduction of iron in the root zone and influences on metal mobility. In: Violante, A.; Huang, PM.; Gadd, GM., editors. Biophysico-Chemical Processes of Heavy Metals and Metalloids in Soil Environments. John Wiley & Sons; New Jersey, USA: 2008. p. 339-371.

Ottonello G, Vetuschi Zuccolini M. The iron-isotope fractionation dictated by the carboxylic functional: An ab-initio investigation. Geochim Cosmochim Acta 2008;72:5920–5934.

Polyakov VB, Mineev SD. The use of Mössbauer spectroscopy in stable isotope geochemistry. Geochim Cosmochim Acta 2000;64:849–865.

Poulson RL, Johnson CM, Beard BL. Iron isotope exchange kinetics at the nanoparticulate ferrihydrite surface. American Mineralogist 2005;90(4):758–763.

Schaedler S, Burkhardt C, Hegler F, Straub KL, Miot J, Benzerara K, Kappler A. Formation of cell-iron-mineral aggregates by phototrophic and nitrate-reducing anaerobic Fe(II)-oxidizing bacteria. Geomicrobiol J 2009;26:93–103.

Schaedler S, Burkhardt C, Kappler A. Evaluation of electron microscopic sample preparation methods and imaging techniques for characterization of cell-mineral aggregates. Geomicrobiol J 2008;25:228–239.

Schauble EA, Rossman GR, Taylor HP. Theoretical estimates of equilibrium Fe-isotope fractionations from vibrational spectroscopy. Geochim Cosmochim Acta 2001;65(15):2487–2497.

Schwertmann, U.; Cornell, RM. Iron oxides in the laboratory. 2. Wiley; 2000.

Skulan JL, Beard BL, Johnson CM. Kinetic and equilibrium Fe isotope fractionation between aqueous Fe(III) and hematite. Geochim Cosmochim Acta 2002;66(17):2995–3015.

Sobolev D, Roden EE. Suboxic deposition of ferric iron by bacteria in opposing gradients of Fe(II) and oxygen at circumneutral pH. Appl Environ Microbiol 2001;67(3):1328–1334. [PubMed: 11229928]

Stookey LL. Ferrozine-a new spectrophotometric reagent for iron. Anal Chem 1970;42:779–781.

Straub KL, Benz M, Schink B, Widdel F. Anaerobic, nitrate-dependent microbial oxidation of ferrous iron. Appl Environ Microbiol 1996;62:1458–1460. [PubMed: 16535298]

Stumm, W.; Morgan, JJ. Aquatic chemistry: chemical equilibria and rates in natural waters. Wiley-Interscience; 1995. p. 1040

Zachara JM, Fredrickson JK, Smith SC, Gassman PL. Solubilization of Fe(III) oxide-bound trace metals by a dissimilatory Fe(III) reducing bacterium. Geochim Cosmochim Acta 2001;65:75–93.

Weber KA, Achenbach LA, Coates JD. Microorganisms pumping iron: anaerobic microbial iron oxidation and reduction. Nature 2006;4:752–764.

Welch SA, Beard BL, Johnson CM, Braterman PS. Kinetic and equilibrium Fe isotope fractionation between aqueous Fe(II) and Fe(III). Geochim Cosmochim Acta 2003;67(22):4231–4250.

Widdel F, Schnell S, Heising S, Ehrenreich A, Assmus B, Schink B. Ferrous iron oxidation by anoxygenic phototrophic bacteria. Nature 1993;362:834–836.

Wiesli RA, Beard BL, Johnson CM. Experimental determination of Fe isotope fractionation between aqueous Fe(II), siderite and “green rust” in abiotic systems. Chem Geol 2004;211:343–362.

Wu L, Beard BL, Roden EE, Johnson CM. Influence of pH and dissolved Si on Fe isotope fractionation during dissimilatory microbial reduction of hematite. Geochim Cosmochim Acta 2009;73:5584–5599.

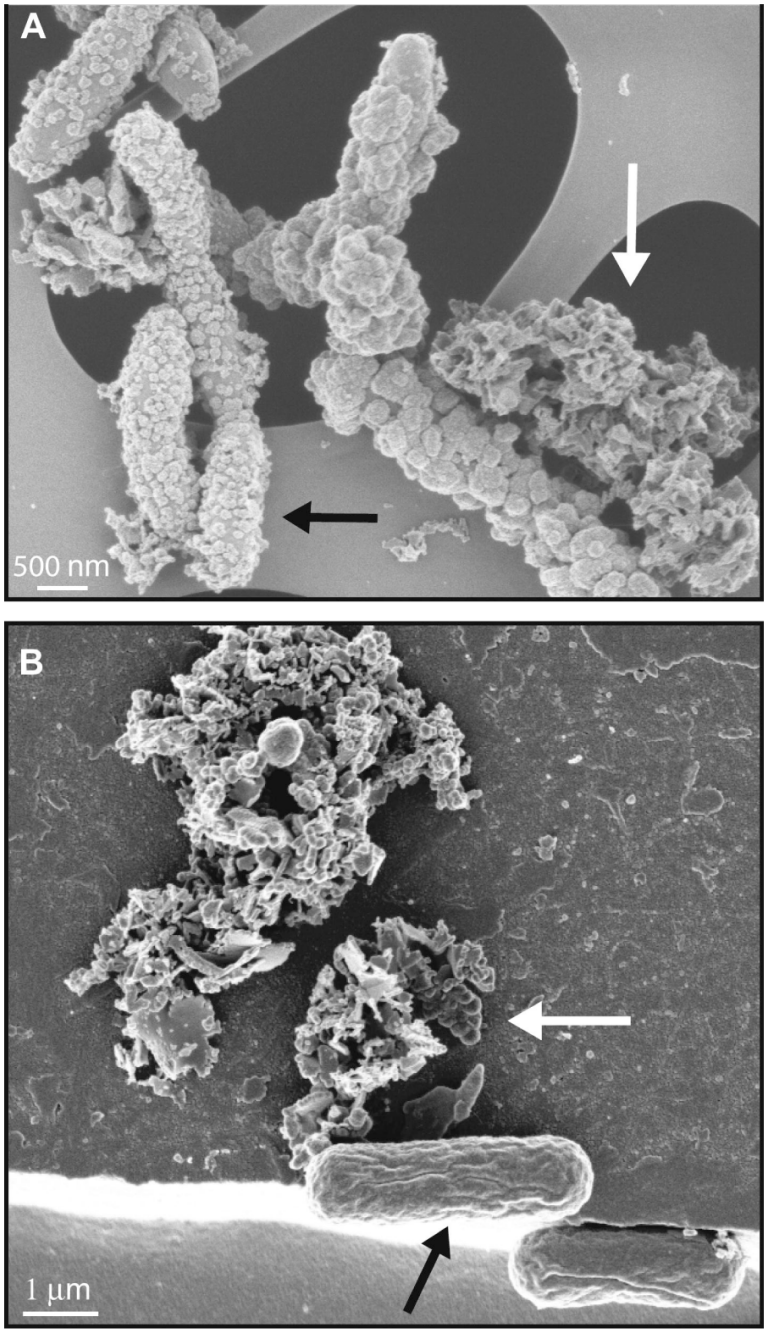

Fig. 1.

Comparison of scanning electron micrographs of circum-neutral pH Fe(II)-oxidizing bacteria. A) Nitrate-reducing Fe(II)-oxidizing *Acidovorax* sp. strain BoFeN1 cells heavily encrusted in iron(III) (hydr)oxides (black arrow) plus extracellular Fe(III) mineral precipitates (filaments – white arrow). B) Phototrophic Fe(II)-oxidizer *Thiodictyon* sp. strain F4 (black arrow) associated with, but not encrusted in iron(III) (hydr)oxides (white arrow). *Thiodictyon* sp. strain F4 was used in the Fe-isotope study of phototrophic Fe(II)-oxidizers by Croal et al. (2004).

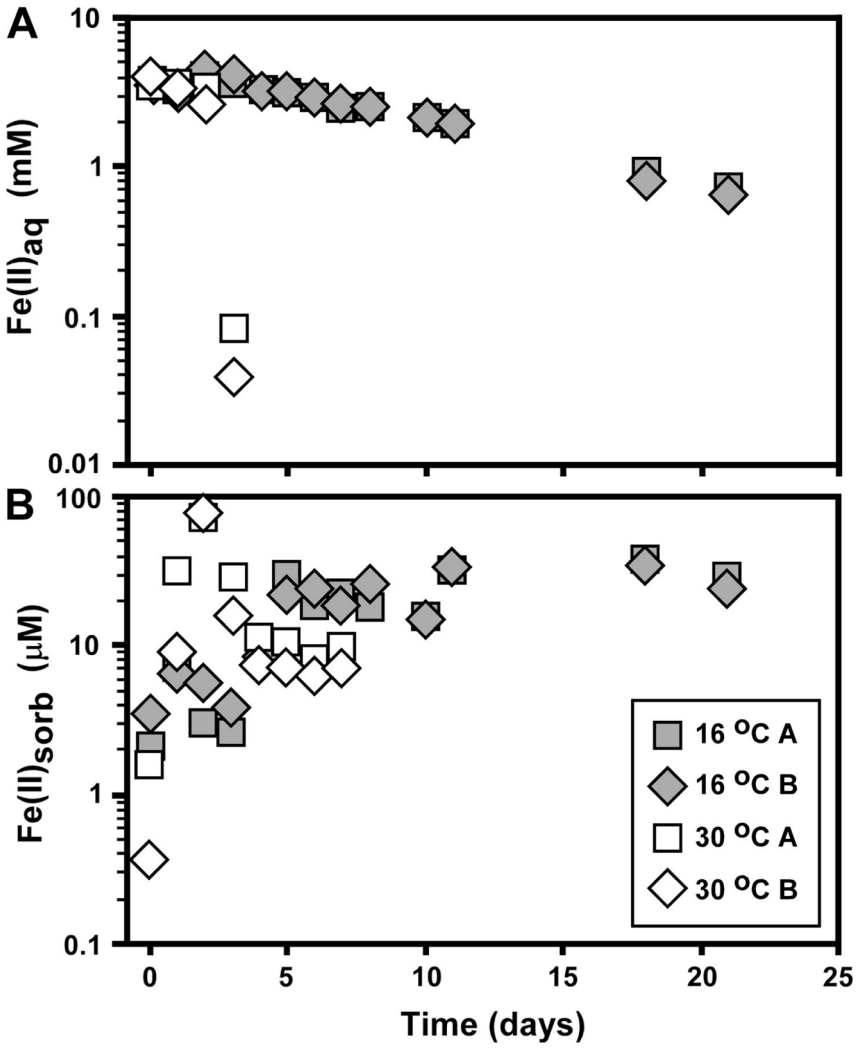

Fig. 2.

Temporal changes in aqueous Fe(II) (A) and sorbed Fe(II) (B) during Fe(II) oxidation by the nitrate-reducing bacterium *Acidovorax* sp. strain BoFeN1 at 16°C and 30°C. Symbols for sorbed Fe plotted as average of two extractions (Table 1). Data for uninoculated controls not shown (see Table 1).

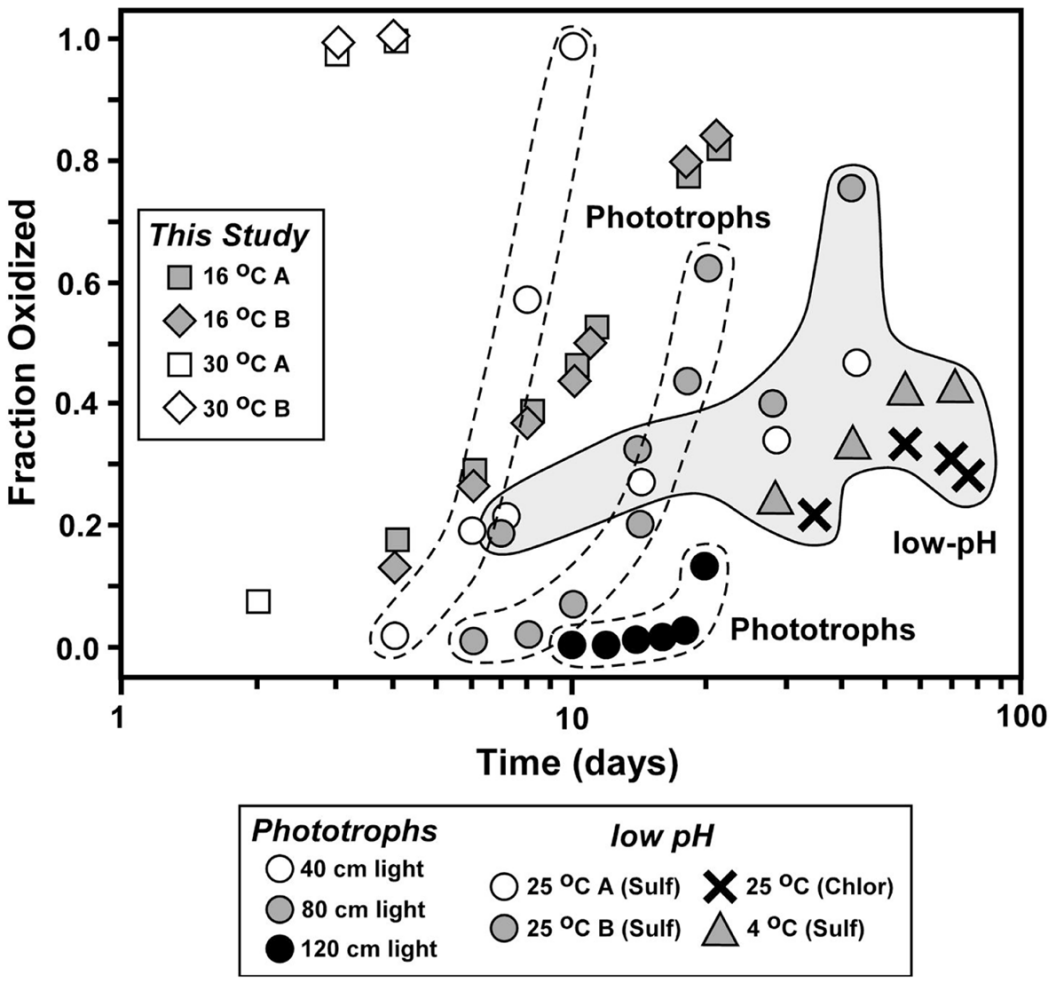

Fig. 3.

Comparison of oxidation rates measured in microbial experiments in the current study of *Acidovorax* sp. strain BoFeN1 (Table 1), Fe(II)-oxidizing phototrophs at circumneutral pH (Croal et al., 2004), and low-pH Fe(II)-oxidizing bacteria (Balci et al., 2006). The study of Croal et al. (2004) was conducted at room temperature, whereas those of Balci et al. (2006) and the current work were conducted at different temperatures, as noted.

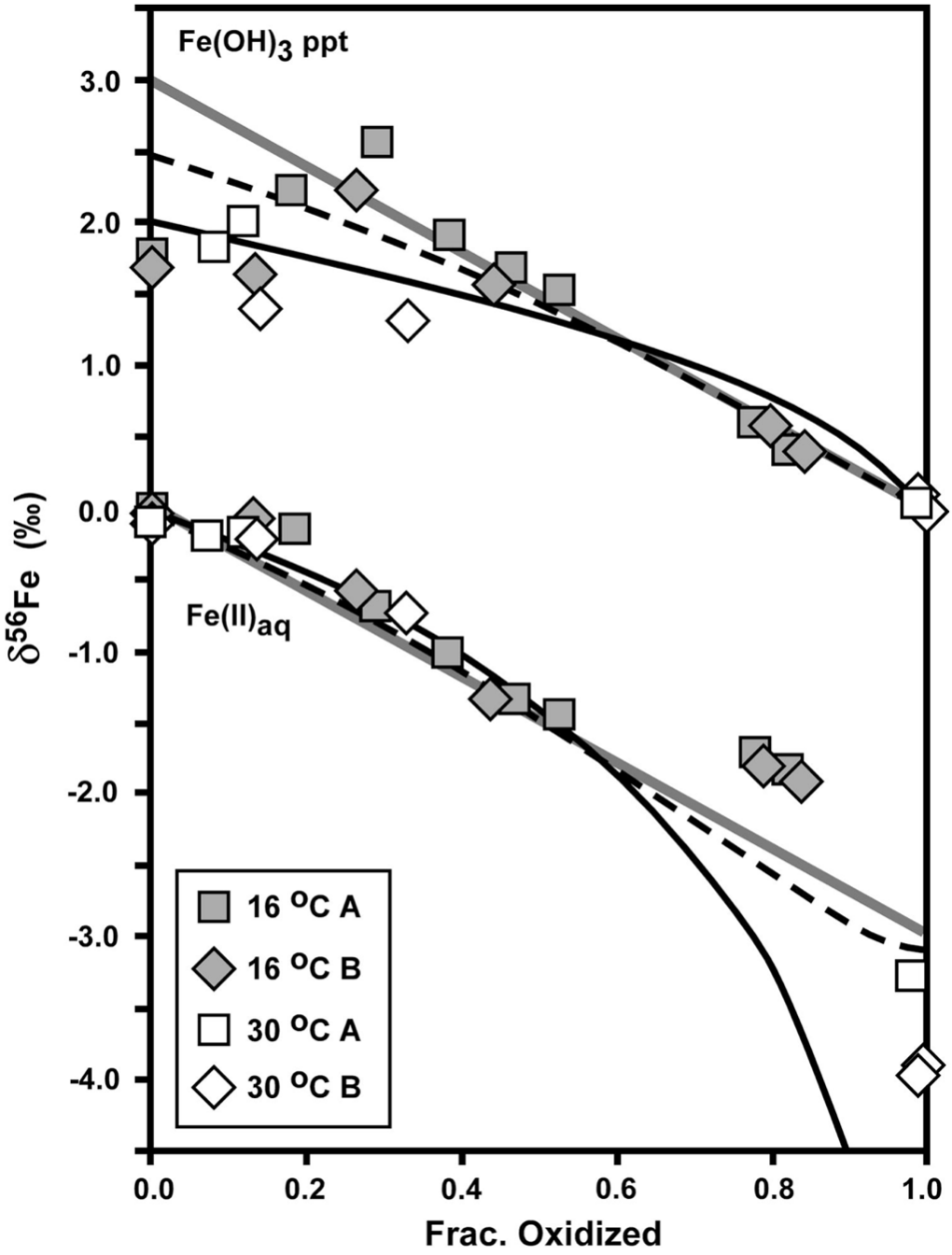

Fig. 4.

Isotopic data for $Fe(II)_{aq}$ and $Fe(OH)_3$ precipitate produced by Fe(II) oxidation by *Acidovorax* sp. strain BoFeN1, as a function of fraction oxidized (Table 1). $\delta^{56}Fe$ values normalized to a system value of zero. Reference curves shown for a) Rayleigh fractionation using a net $\Delta^{56}Fe_{Fe(OH)3 - Fe(II)aq}$ fractionation of +2 ‰ (black curve), b) the Rayleigh fractionation curve modified to account for partial isotopic re-equilibration (dashed black curve), and c) closed-system equilibrium fractionation for $\Delta^{56}Fe_{Fe(OH)3 - Fe(II)aq}$ = +3 ‰ (straight grey line). Partial isotopic re-equilibration calculated assuming a reactive Fe(III) surface layer of 1 nm thickness (10 nm diameter spherical particle) maintains isotopic equilibrium with $Fe(II)_{aq}$. $\delta^{56}Fe$ value for $Fe(II)_{aq}$ calculated in the partial re-equilibration

model at increments of 1 % oxidation, using the isotope mass balance equation (eq. 4) from Crosby et al. (2007), modified to ignore sorbed Fe(II).

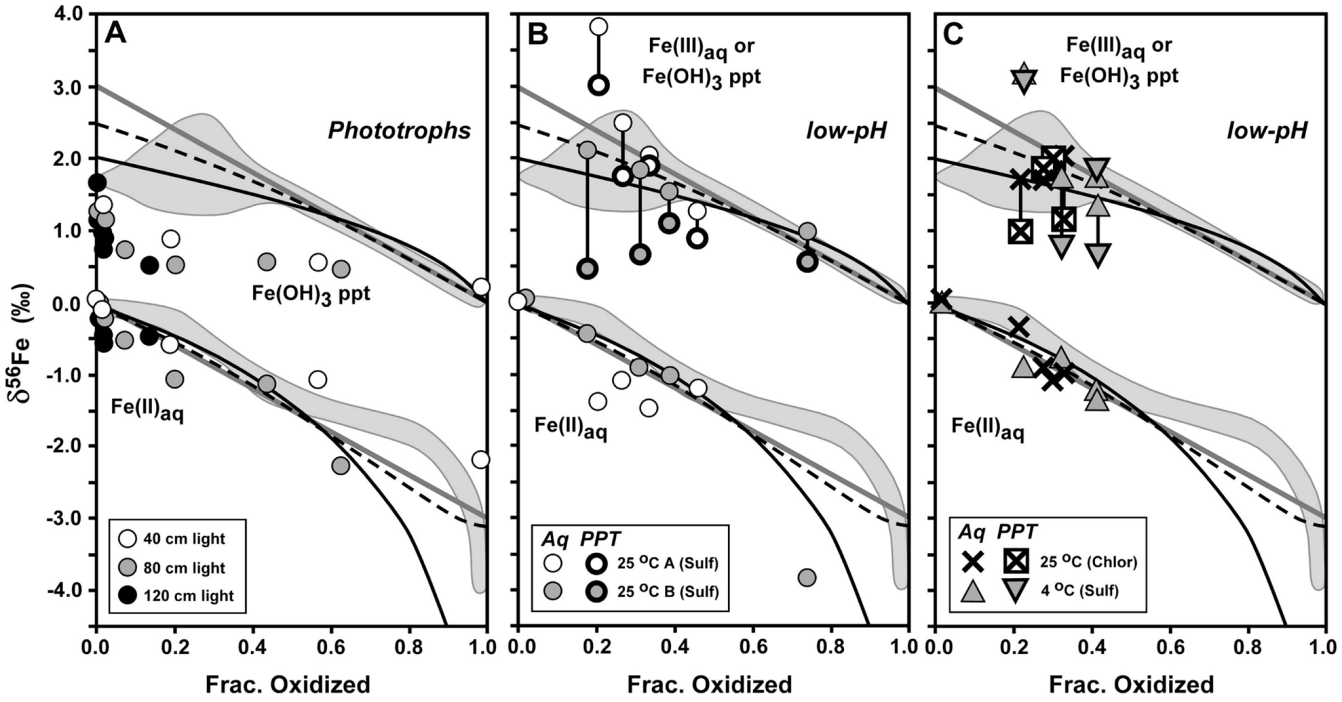

Fig. 5.

Comparison of Fe isotope variations of the current study (grey fields, from Fig. 4) with phototrophic Fe(II) oxidation (panel A, from Croal et al., 2004) and low-pH Fe(II) oxidation (panels B and C, from Balci et al., 2006). $\delta^{56}Fe$ values normalized to a system value of zero for all studies to allow direct comparison. Reference curves shown from Fig. 4 for a) Rayleigh fractionation using a net $\Delta^{56}Fe_{Fe(OH)3 - Fe(II)aq}$ fractionation of +2 ‰ (black curve), b) the Rayleigh fractionation curve modified to account for partial isotopic re-equilibration (dashed black curve), and c) closed-system equilibrium fractionation for $\Delta^{56}Fe_{Fe(OH)3 - Fe(II)aq}$ = +3 ‰ (straight grey line). For low-pH experiments of Balci et al. (2006) (panels B and C), $\delta^{56}Fe$ values for aqueous Fe(III) and Fe(II) shown with thin line for symbols, and $\delta^{56}Fe$ values for ferric hydroxide precipitates shown with thick line for symbols.

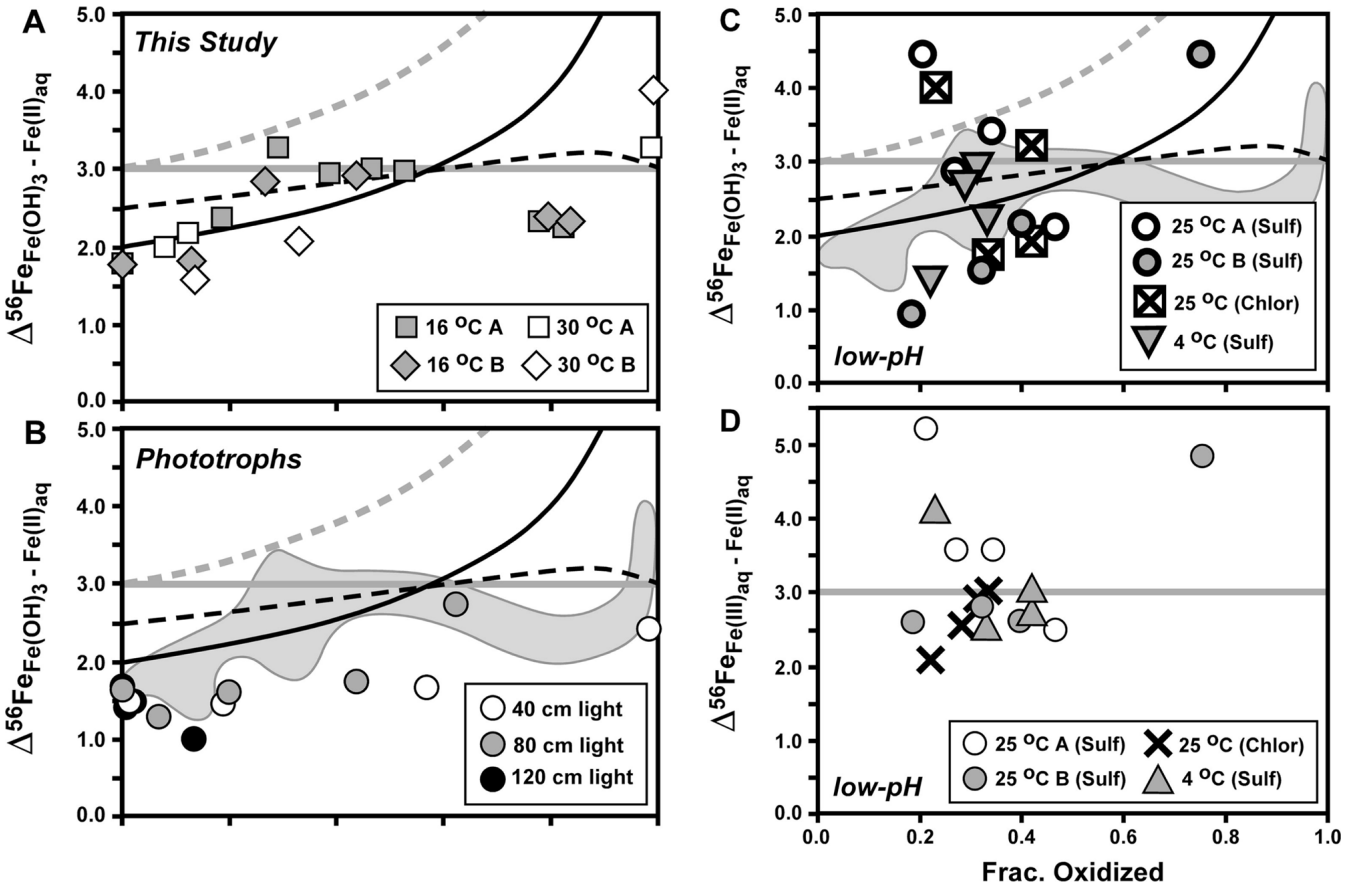

Fig. 6.

Comparison of isotopic fractionations between ferric hydroxide precipitate ($Fe(OH)_3$) and $Fe(II)_{aq}$ (panel A: current study (Table 1); panel B: study of Croal et al., 2004; panel C: study of Balci et al., 2006), as well as between $Fe(III)_{aq}$ and $Fe(II)_{aq}$ from the study of Balci et al. (2006) (panel D). Reference curves for panels A–C shown from Figs. 4 and 5 for Rayleigh fractionation using a net $\Delta^{56}Fe_{Fe(OH)3 - Fe(II)aq}$ fractionation of +2 ‰ (black curve), the Rayleigh fractionation curve modified to account for partial isotopic re-equilibration (dashed black curve), and closed-system equilibrium fractionation for $\Delta^{56}Fe_{Fe(OH)3 - Fe(II)aq}$ = +3 ‰ (straight grey line). In addition, a Raleigh curve for an equilibrium $\Delta^{56}Fe_{Fe(III)aq - Fe(II)aq}$ fractionation of +3 ‰, followed by quantitative sequestration of $Fe(III)_{aq}$ to $Fe(OH)_3$, is shown in grey dashed line (panels A–C). Reference curve for closed-system equilibrium fractionation for $\Delta^{56}Fe_{Fe(III)aq - Fe(II)aq}$ = +3 ‰ (straight grey line) shown for panel D. Grey field in panels B and C shows outline of data from panel A.

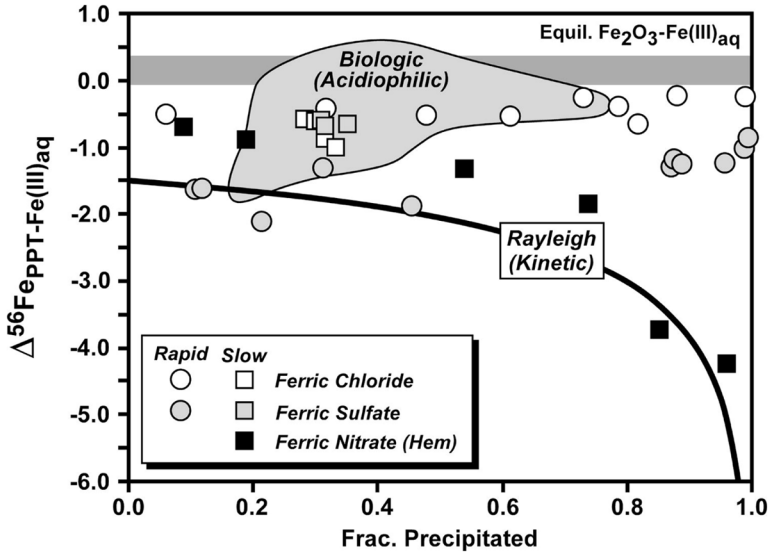

Fig. 7.

Compilation of fractionations measured between ferric oxide/hydroxide and $Fe(III)_{aq}$ from the studies of Skulan et al. (2002) and Balci et al. (2006). Skulan et al. estimated a slightly positive equilibrium hematite – $Fe(III)_{aq}$ fractionation at 98 °C (horizontal dark grey field, and determined a kinetic hematite – $Fe(III)_{aq}$ fractionation at 98°C (black squares) that can be described by a Rayleigh process and a $\Delta^{56}Fe_{Hematite - Fe(III)aq}$ fractionation between −1 and −1.5 ‰ (black curve shown for −1.5 ‰). The fractionation between ferric hydroxide precipitates and co-existing $Fe(III)_{aq}$ shown for abiologic precipitation experiments (symbols) and measured in biologic oxidation experiments (light grey field) also shown from the study of Balci et al. (2006).

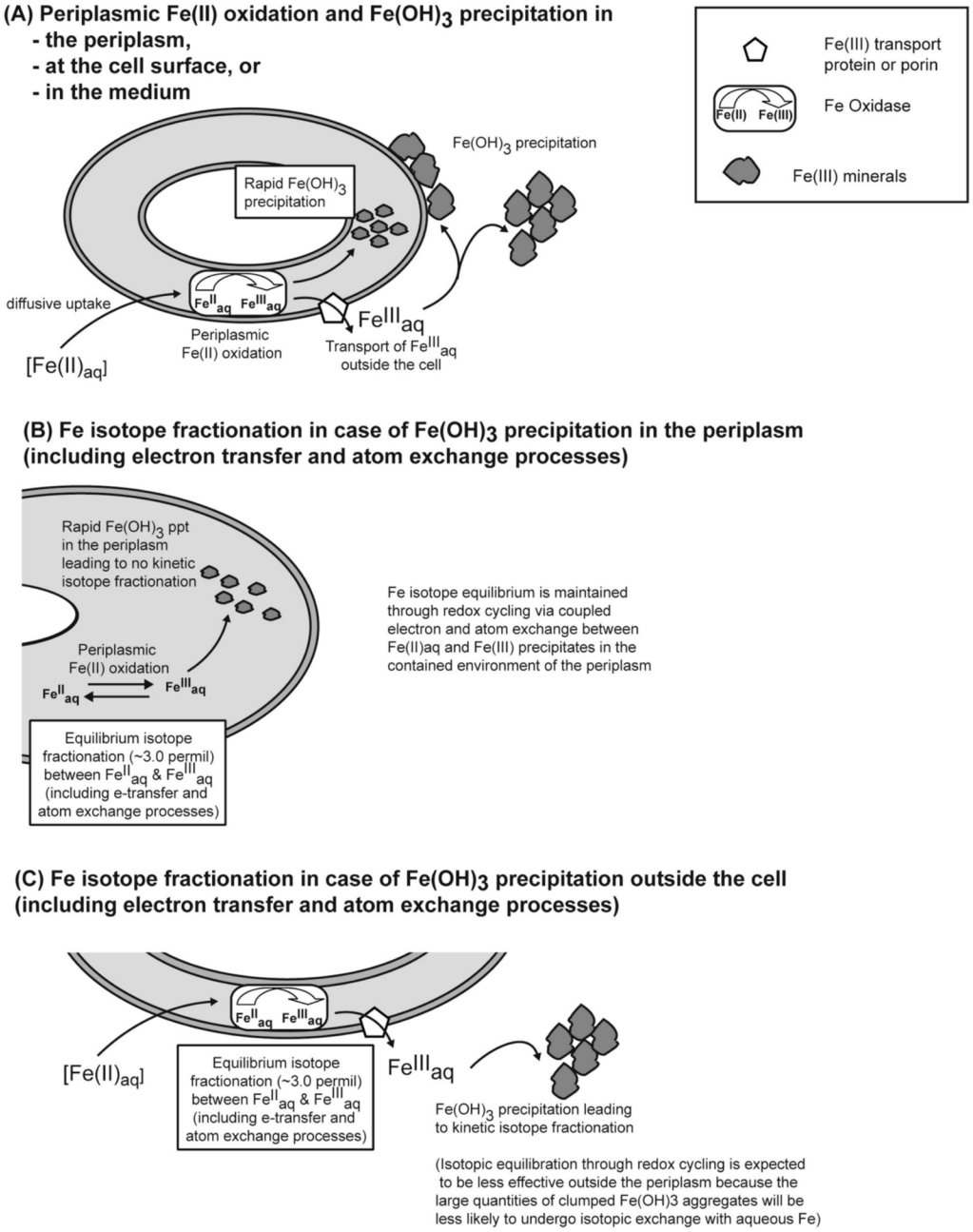

Fig. 8.

Cartoon illustrating periplasmic oxidation of Fe(II) by *Acidovorax* sp. strain BoFeN1 followed by $Fe(OH)_3$ precipitation either in the periplasm, at the cell surface or extracellularly (A) and potential Fe isotope fractionations expected in case of periplasmic (B) and extracellular (C) Fe $(OH)_3$ precipitation.

Table 1

Concentration and isotopic data. The data is given for two (abiotic, i.e. cell-free) control bottles A and B as well as for two bottles (A and B each) for Fe(II)-oxidizing *Acidovorax* cultures grown at 16°C and 30°C (labelling #1 – #18 represents different time points (in days) of sampling.

Sample	Day	Fe(II) mM	Percent oxidation	Analysis	δ^{56}Fe	2SE/1SD	δ^{57}Fe	2SE/1SD
Control - Bottle A								
CtrlA-#0-1 Aq	0	3.94		1	0.33 ±	0.06	0.54 ±	0.08
				2	0.33 ±	0.07	0.54 ±	0.04
				Avg	0.33 ±	0.00	0.54 ±	0.00
CtrlA-#1-1 Aq	1	3.65						
CtrlA-#2-1 Aq	2	4.46		1	0.40 ±	0.07	0.59 ±	0.07
				2	0.36 ±	0.04	0.53 ±	0.02
				Avg	0.38 ±	0.03	0.56 ±	0.04
CtrlA-#3-1 Aq	3	4.10						
CtrlA-#4-1 Aq	4	4.27		1	0.40 ±	0.06	0.57 ±	0.09
				2	0.34 ±	0.04	0.54 ±	0.03
				Avg	0.37 ±	0.05	0.55 ±	0.03
CtrlA-#5-1 Aq	5	4.03						
CtrlA-#6-1 Aq	6	4.14		1	0.28 ±	0.06	0.44 ±	0.07
				2	0.41 ±	0.05	0.62 ±	0.08
				3	0.28 ±	0.04	0.44 ±	0.03
				Avg	0.32 ±	0.07	0.50 ±	0.10
CtrlA-#7-1 Aq	7	4.07						
CtrlA-#8-1 Aq	8	4.07						
CtrlA-#10-1 Aq	10	4.00						
CtrlA-#11-1 Aq	11	4.15						
CtrlA-#18-1 Aq	18	4.19						
Control - Bottle B								
CtrlB-#0-1 Aq	0	4.08						
CtrlB-#1-1 Aq	1	3.55						
CtrlB-#2-1 Aq	2	4.03						
CtrlB-#3-1 Aq	3	3.71						
CtrlB-#4-1 Aq	4	4.21						

Sample	Day	Fe(II) mM	Percent oxidation	Analysis	δ^{56}Fe	2SE/1SD	δ^{57}Fe	2SE/1SD
CtrlB-#5-1 Aq	5	3.87						
CtrlB-#6-1 Aq	6	4.21						
CtrlB-#7-1 Aq	7	4.01						
CtrlB-#8-1 Aq	8	4.12						
CtrlB-#10-1 Aq	10	4.00						
CtrlB-#11-1 Aq	11	4.20						
CtrlB-#18-1 Aq	18	4.29						
Bottle 16A - 16 °C								
16A-#0-1 Aq	0	3.54	0.0	1	0.32 ±	0.04	0.41 ±	0.06
				2	0.34 ±	0.04	0.65 ±	0.08
				Avg	0.33 ±	0.02	0.53 ±	0.17
16A-#0-1 Sorb		0.0021						
16A-#1-1 Aq	1	3.11	0.0					
16A-#1-1 Sorb		0.0070						
16A-#2-1 Aq	2	3.89	0.0	1	0.30 ±	0.04	0.48 ±	0.04
				2	0.24 ±	0.04	0.30 ±	0.05
				Avg	0.27 ±	0.04	0.39 ±	0.13
16A-#2-1 Sorb		0.0030						
16A-#2-1 Precip				1	2.08 ±	0.05	3.18 ±	0.04
16A-#3-1 Aq	3	3.60	7.4					
16A-#3-1 Sorb		0.0026						
16A-#4-1 Aq	4	3.19	17.8	1	0.18 ±	0.04	0.27 ±	0.05
				2	0.20 ±	0.05	0.21 ±	0.07
				Avg	0.19 ±	0.02	0.24 ±	0.05
16A-#4-1 Sorb		0.0085						
16A-#4-1 Precip				1	2.60 ±	0.05	4.07 ±	0.08
				2	2.53 ±	0.03	3.89 ±	0.04
				Avg	2.56 ±	0.05	3.98 ±	0.13
16A-#5-1 Aq	5	3.03	21.4					
16A-#5-1 Sorb		0.0294						
16A-#6-1 Aq	6	2.77	28.3	1	−0.33 ±	0.08	−0.57 ±	0.08
				2	−0.35 ±	0.04	−0.61 ±	0.06

Sample	Day	Fe(II) mM	Percent oxidation	Analysis	δ^{56}Fe	2SE/1SD	δ^{57}Fe	2SE/1SD
				Avg	−0.34 ±	0.01	−0.59 ±	0.02
16A-#6-1 Sorb		0.0176						
16A-#6-1 Precip				1	2.84 ±	0.07	4.40 ±	0.11
				2	2.98 ±	0.02	4.51 ±	0.03
				Avg	2.91 ±	0.10	4.46 ±	0.08
16A-#7-1 Aq	7	2.41	37.5					
16A-#7-1 Sorb		0.0221						
16A-#8-1 Aq	8	2.40	37.8	1	−0.70 ±	0.06	−1.02 ±	0.08
				2	−0.64 ±	0.04	−0.89 ±	0.06
				Avg	−0.67 ±	0.04	−0.96 ±	0.09
16A-#8-1 Sorb		0.0183						
16A-#8-1 Precip				1	2.27 ±	0.04	3.37 ±	0.03
				2	2.25 ±	0.04	3.38 ±	0.03
				Avg	2.26 ±	0.02	3.37 ±	0.01
16A-#9-1 Aq	10	2.10	45.6	1	−0.98 ±	0.04	−1.44 ±	0.04
16A-#9-1 Sorb		0.0160						
16A-#9-1 Precip				1	2.01 ±	0.03	2.96 ±	0.05
16A-#10-1 Aq	11	1.86	51.4	1	−1.13 ±	0.05	−1.66 ±	0.08
				2	−1.08 ±	0.03	−1.61 ±	0.03
				Avg	−1.10 ±	0.04	−1.64 ±	0.04
16A-#10-1 Sorb		0.0307						
16A-#10-1 Precip				1	1.90 ±	0.04	2.81 ±	0.03
				2	1.83 ±	0.07	2.75 ±	0.11
				Avg	1.87 ±	0.05	2.78 ±	0.04
16A-#11-1 Aq	18	0.87	76.7	1	−1.36 ±	0.03	−2.01 ±	0.04
16A-#11-1 Sorb		0.0358						
16A-#11-1 Precip				1	0.95 ±	0.05	1.44 ±	0.04
16A-#12-1 Aq	21	0.70	81.3	1	−1.48 ±	0.04	−2.14 ±	0.04
16A-#12-1 Sorb		0.0285						
16A-#12-1 Precip				1	0.76 ±	0.05	1.04 ±	0.08
Bottle 16B - 16 °C								
16B-#0-1 Aq	0	3.85	0.0	1	0.30 ±	0.03	0.48 ±	0.07

Geochim Cosmochim Acta. Author manuscript; available in PMC 2010 November 10.

Sample	Day	Fe(II) mM	Percent oxidation	Analysis	δ^{56}Fe	2SE/1SD	δ^{57}Fe	2SE/1SD
16B-#0-1 Sorb		0.0038						
16B-#0-1 Precip				1	2.02 ±	0.04	2.96 ±	0.06
16B-#1-1 Aq	1	3.43	10.7					
16B-#1-1 Sorb		0.0089						
16B-#2-1 Aq	2	3.84	0.1	1	0.27 ±	0.05	0.37 ±	0.04
16B-#2-1 Sorb		0.0059						
16B-#2-1 Precip				1	2.06 ±	0.05	3.18 ±	0.05
				2	2.09 ±	0.05	3.16 ±	0.04
				Avg	2.08 ±	0.03	3.17 ±	0.01
16B-#3-1 Aq	3	4.14	0.0					
16B-#3-1 Sorb		0.0039						
16B-#4-1 Aq	4	3.35	12.7	1	0.17 ±	0.03	0.27 ±	0.03
16B-#4-1 Sorb		0.0104						
16B-#4-1 Precip				1	1.97 ±	0.03	2.96 ±	0.03
16B-#5-1 Aq	5	3.11	18.6					
16B-#5-1 Sorb		0.0224						
16B-#6-1 Aq	6	2.83	25.9	1	−0.24 ±	0.05	−0.31 ±	0.06
				2	−0.27 ±	0.05	−0.39 ±	0.04
				Avg	−0.25 ±	0.02	−0.35 ±	0.06
16B-#6-1 Sorb		0.0239						
16B-#6-1 Precip				1	2.55 ±	0.03	3.79 ±	0.04
16B-#7-1 Aq	7	2.62	31.5					
16B-#7-1 Sorb		0.0180						
16B-#8-1 Aq	8	2.44	35.9					
16B-#8-1 Sorb		0.0261						
16B-#9-1 Aq	10	2.17	43.2	1	−1.00 ±	0.05	−1.41 ±	0.04
16B-#9-1 Sorb		0.0152						
16B-#9-1 Precip				1	1.90 ±	0.05	2.87 ±	0.06
16B-#10-1 Aq	11	1.93	49.0					
16B-#10-1 Sorb		0.0317						
16B-#11-1 Aq	18	0.78	78.9	1	−1.50 ±	0.03	−2.24 ±	0.04
				2	−1.43 ±	0.05	−2.14 ±	0.04

Sample	Day	Fe(II) mM	Percent oxidation	Analysis	δ^{56}Fe	2SE/1SD	δ^{57}Fe	2SE/1SD
				Avg	−1.46 ±	0.05	−2.19 ±	0.07
16B-#11-1 Sorb		0.0340						
16B-#11-1 Precip				1	0.91 ±	0.03	1.32 ±	0.03
16B-#12-1 Aq	21	0.63	83.0	1	−1.56 ±	0.03	−2.28 ±	0.07
16B-#12-1 Sorb		0.0239						
16B-#12-1 Precip				1	0.75 ±	0.03	1.07 ±	0.03
Bottle 30A - 30 °C								
30A-#0-1 Aq	0	3.73	0.0	1	0.31 ±	0.04	0.37 ±	0.06
				2	0.32 ±	0.05	0.59 ±	0.06
				Avg	0.32 ±	0.01	0.48 ±	0.15
30A-#0-1 Sorb		0.0016						
30A-#1-1 Aq	1	3.30	10.7	1	0.19 ±	0.05	0.25 ±	0.05
30A-#1-1 Sorb		0.0314						
30A-#1-1 Precip				1	2.38 ±	0.07	3.45 ±	0.04
				2	2.31 ±	0.04	3.35 ±	0.04
				Avg	2.35 ±	0.05	3.40 ±	0.07
30A-#2-1 Aq	2	3.46	5.3	1	0.14 ±	0.04	0.11 ±	0.07
				2	0.15 ±	0.03	0.20 ±	0.03
				Avg	0.15 ±	0.01	0.16 ±	0.07
30A-#2-1 Sorb		0.0715						
30A-#2-1 Precip				1	2.23 ±	0.03	3.30 ±	0.05
				2	2.10 ±	0.04	3.11 ±	0.04
				Avg	2.17 ±	0.09	3.20 ±	0.13
30A-#3-1 Aq	3	0.08	97.1	1	−2.91 ±	0.05	−4.18 ±	0.04
				2	−2.91 ±	0.07	−4.37 ±	0.05
				Avg	−2.91 ±	0.00	−4.28 ±	0.13
30A-#3-1 Sorb		0.0280						
30A-#3-1 Precip				1	0.42 ±	0.08	0.62 ±	0.11
				2	0.37 ±	0.04	0.55 ±	0.03
				Avg	0.39 ±	0.03	0.58 ±	0.05
30A-#4-1 Precip	4			1	0.41 ±	0.04	0.59 ±	0.03
				2	0.39 ±	0.03	0.51 ±	0.06

Sample	Day	Fe(II) mM	Percent oxidation	Analysis	δ^{56}Fe	2SE/1SD	δ^{57}Fe	2SE/1SD
				3	0.30 ±	0.09	0.34 ±	0.09
				Avg	0.36 ±	0.06	0.48 ±	0.12
Bottle 30B - 30 °C								
30B-#0-1 Aq	0	3.94	0.0	1	0.25 ±	0.03	0.32 ±	0.05
30B-#0-1 Sorb		0.0004						
30B-#1-1 Aq	1	3.41	13.2	1	0.17 ±	0.03	0.23 ±	0.04
30B-#1-1 Sorb		0.0094						
30B-#1-1 Precip				1	1.75 ±	0.04	2.63 ±	0.04
30B-#2-1 Aq	2	2.64	30.8	1	−0.39 ±	0.02	−0.56 ±	0.04
30B-#2-1 Sorb		0.0864						
30B-#2-1 Precip				1	1.67 ±	0.08	2.49 ±	0.04
30B-#3-1 Aq	3	0.04		1	−3.56 ±	0.03	−5.20 ±	0.03
				2	−3.61 ±	0.05	−5.29 ±	0.04
				Avg	−3.59 ±	0.04	−5.25 ±	0.06
30B-#3-1 Sorb		0.0016						
30B-#3-1 Precip				1	0.44 ±	0.04	0.66 ±	0.05
30B-#4-1 Precip	4			1	0.33 ±	0.04	0.48 ±	0.03
				2	0.32 ±	0.04	0.47 ±	0.04
				Avg	0.33 ±	0.00	0.48 ±	0.01